Title

Targeting the PSGL-1 Immune Checkpoint Promotes Immunity to PD-1-Resistant Melanoma.

Journal

Cancer Immunology Research, 10(5)

ISSN

2326-6066

Authors

DeRogatis, Julia M
Viramontes, Karla M
Neubert, Emily N
et al.

Publication Date

2022-05-03

DOI

10.1158/2326-6066.cir-21-0690

Peer reviewed

HHS Public Access

Author manuscript

Cancer Immunol Res. Author manuscript; available in PMC 2022 November 03.

Published in final edited form as:

Cancer Immunol Res. 2022 May 03; 10(5): 612–625. doi:10.1158/2326-6066.CIR-21-0690.

Targeting the PSGL-1 Immune Checkpoint Promotes Immunity to PD-1 Resistant Melanoma

Julia M. DeRogatis[1], **Karla M. Viramontes**[1,7], **Emily N. Neubert**[1,7], **Monique L. Henriquez**[1], **Christian F. Guerrero-Juarez**[2,3,4,5,6], **Roberto Tinoco**[1,*]

[1]Department of Molecular Biology and Biochemistry, School of Biological Sciences, University of California, Irvine, CA 92697, USA

[2]Department of Developmental and Cell Biology, University of California, Irvine, CA 92697, USA

[3]Sue and Bill Gross Stem Cell Research Center, University of California, Irvine, CA 92697, USA

[4]Department of Mathematics, University of California, Irvine, CA, 92697, USA

[5]Center for Complex Biological Systems, University of California, Irvine, CA 92697, USA

[6]NSF-Simons Center for Multiscale Cell Fate Research, University of California, Irvine, CA, 92697, USA

[7]Contributed equally

Abstract

Immune checkpoint inhibitors have had impressive efficacy in some cancer patients, reinvigorating long-term durable immune responses against tumors. Despite the clinical success of these therapies, most cancer patients continue to be unresponsive to these treatments, highlighting the need for novel therapeutic options. Although P-selectin glycoprotein ligand-1 (PSGL-1) has been shown to inhibit immune responses in a variety of disease models, previous work has yet to address whether PSGL-1 can be targeted therapeutically to promote antitumor immunity. Using an aggressive melanoma tumor model, we targeted PSGL-1 in tumor-bearing mice and found increased effector $CD4^+$ and $CD8^+$ T-cell responses and decreased regulatory T cells (Tregs) in tumors. T cells exhibited increased effector function, activation, and proliferation, which delayed tumor growth in mice after anti-PSGL-1 treatment. Targeting PD-1 in PSGL-1-deficient, tumor-bearing mice led to an increased frequency of mice with complete tumor eradication. Targeting both PSGL-1 and PD-1 in wild-type tumor-bearing mice also showed enhanced anti-tumor immunity and slowed melanoma tumor growth. Our findings showed that therapeutically targeting the PSGL-1 immune checkpoint can reinvigorate anti-tumor immunity and suggest that targeting PSGL-1 may represent a new therapeutic strategy for cancer treatment.

[*]**Correspondence:** Roberto Tinoco, 3244 McGaugh Hall, Irvine, CA 92697, (949) 824-4926, rtinoco@uci.edu.

AUTHOR CONTRIBUTIONS

R.T. conceived, directed and obtained funding for the project. J.M.D. and R.T. conceptualized, designed and analyzed the experiments and wrote the manuscript. J.M.D., K.M.V., E.N.N. and M.L.H. performed the experiments. J.M.D., K.M.V., E.N.N. and M.L.H. performed anti-PSGL-1 experiments, E.N.N. performed experiments in *Selplg*$^{-/-}$ mice, M.L.H. helped with the T cell depletion antibody blockade experiments. C.F.G-J. helped analyze and interpret scRNA-seq data. All authors provided feedback and approved the manuscript.

The authors declare no potential conflicts of interest.

Keywords

PSGL-1; PD-1; Immune Checkpoint Inhibitors; Melanoma; Immunotherapy

INTRODUCTION

Immune checkpoint inhibitors have revolutionized the treatment of many cancer types, including melanoma, and are now standard-of-care (1,2). Blocking the PD-1/PD-L1 and CTLA-4 pathway in melanoma has shown efficacy in patients through the reinvigoration of anti-tumor T cells (3,4). Although these immune checkpoint inhibitors show significant clinical success in multiple cancer types, most patients with melanoma remain unresponsive, and many develop immune-related adverse events (irAEs)(2,5–8). Immune checkpoints in melanoma actively suppress T cells to induce an exhausted dysfunctional state, which promotes tumor growth and metastasis (9). The high expression of these immune checkpoints on exhausted T cells diminishes their effector functions and cytotoxicity (10). Although PD-1 and CTLA-4 have been well studied, additional immune checkpoints have been identified that also promote T-cell exhaustion, including P-selectin glycoprotein ligand-1 (PSGL-1)(11).

Most tumor-infiltrating leukocytes involved in the immune response express PSGL-1 (12–14). Although T cells utilize PSGL-1 for migration through selectin interactions, PSGL-1 binds additional molecules, such as Siglecs, chemokines, and the recently identified ligand, VISTA (V-domain Ig suppressor of T-cell activation)(15–18). PSGL-1 and selectin-mediated migration have been extensively studied; however, less is known regarding PSGL-1 engagement in the tumor microenvironment, and whether these interactions promote T-cell exhaustion (19). Much of what is known regarding PSGL-1 immune inhibitory function has relied on the use of PSGL-1-deficient mice (*Selplg*$^{-/-}$)(20). Studies have shown that *Selplg*$^{-/-}$ mice develop autoimmunity involving the skin, lungs, and kidneys (21). In addition, *Selplg*$^{-/-}$ mice are shown to develop glomerulonephritis in lupus-prone mice, scleroderma, ulcerative colitis, and experimental autoimmune encephalomyelitis (22–25). *Selplg*$^{-/-}$ dendritic cells (DCs) are more immunogenic, and PSGL-1 signaling in human monocyte-derived DCs leads to a tolerogenic phenotype that promotes regulatory T-cell (Treg) differentiation (26). Furthermore, *Selplg*$^{-/-}$ mice generate less Tregs in the thymus (26–28). PSGL-1 inhibitory function in T cells is also found during immune responses to viral infections and tumors (11,29). *Selplg*$^{-/-}$ mice are shown to control chronic viral infection and melanoma tumors through increased effector T-cell responses (11), and PSGL-1 is also shown to restrain proliferation of memory T cells during acute viral infection (30). These studies also show that despite lacking PSGL-1 expression, *Selplg*$^{-/-}$ effector T cells efficiently migrate to infected tissues and tumors (11). Together, these studies identify PSGL-1 as an important negative immune regulator that not only facilitates T-cell migration, but also functions as an immune checkpoint in T cells (11,30,31). Although studies using *Selplg*$^{-/-}$ have been important for our understanding of PSGL-1 biology, it has not yet been explored whether PSGL-1 can be therapeutically targeted in wild-type (WT) mice with established aggressive melanoma tumors. Here, we report therapeutic efficacy of targeting the PSGL-1 immune checkpoint *in vivo* in melanoma tumor-bearing mice,

which resulted in delayed tumor growth attributed to enhanced effector T-cell responses. Our findings highlight that targeting the PSGL-1 inhibitory pathway therapeutically is an effective strategy to enhance anti-tumor immunity in melanoma.

MATERIALS AND METHODS

A complete list of reagents used in the study in Suppl. Table S1.

Cell lines

Braf$^{V600E/+}$; *Pten*$^{-/-}$; and *Cdkn2a*$^{-/-}$ mouse melanoma cells (YUMMER1.7) were kindly provided by Marcus Bosenberg (Yale). B16-GP_{33} melanoma cells were kindly provided by Dr. Ananda Goldrath (UCSD). Dartmouth murine mutant malignant melanoma-3A (D4M-3A) were kindly provided by Dr. Francesco Marangoni (UC Irvine). Cell lines were maintained in Corning Dulbecco's modified eagle's medium with 10% fetal bovine serum (FBS) (D4M-3A), Corning Iscove's Modified Dulbecco's medium with 10% FBS and 1% Corning Penicillin-Streptomycin-L-Glutamine (PSG)(for YUMMER1.7), or Corning Iscove's Modified Dulbecco's medium with 10% FBS, 1% (PSG) and 1% geneticin (Gibco) (for B16-GP_{33}). Cell lines were passaged two times per week and underwent a minimum of four passages before injections. To mitigate murine cell line adaptations while in culture, cells were cultured for a maximum of two months *in vitro*. Early passages were frozen down for future use. No additional cell authentication was performed. All cell lines were free of mycoplasma.

Mice and experimental model

All experimental animal procedures were approved by the Institutional Animal Care and Use Committee of University of California, Irvine (AUP-18–148) and complied with all relevant ethical regulations for animal testing and research. C57BL/6J and *Selplg*$^{-/-}$ mice were purchased from the Jackson Laboratory, then bred in SPF facilities. Male mice ≥6 weeks of age were used in experiments. Mouse selection for experiments was not formally randomized or blinded.

For tumor growth experiments, mice were injected subcutaneously (s.c.) with 1×10^6 B16-GP_{33} cells in 200μL of sterile PBS or 1×10^6 D4M-3A cells in 100μL of sterile PBS and designated into treatment groups 8 days post injection (dpi) as described in the next section. B16-GP_{33} tumors were measured by caliper at 8, 10, 12, 14–18 dpi, and mice were euthanized at 18 dpi. B16-GP_{33} tumors were dissected, along with the inguinal tumor-draining lymph nodes. D4M tumors were measured by caliper at 8,10,12, 15, 17–19 dpi, and tumors were dissected out at 19 dpi.

For survival experiments, mice were injected with 1×10^6 B16-GP_{33} cells s.c., and mice with tumors <2000 mm^3 at 18 dpi were designated as surviving. Mice in each treatment group had an average tumor size of 60–100mm^3 at 8 dpi, and mice with tumors exceeding 100 mm^3 at this timepoint were euthanized. For the YUMMER1.7 study, mice were s.c. injected with 2×10^6 YUMMER1.7 tumor cells in 200 μL sterile PBS. Tumor size was measured by caliper three times per week and tumors were dissected at 34 or 38 dpi. In YUMMER1.7 experiments with T-cell depleting antibodies, tumors were measured three times per week

and dissected at 21 or 28 dpi. Tumors were weighed at the time of excision. Mice that initially had tumors >40 mm^3 at 8 dpi and then had no palpable tumors following antibody treatment were considered to be complete responders (CR).

In vivo antibody treatments

All monoclonal antibodies for *in vivo* use were from BioXcell (New Hampshire, USA). For antibody treatments, mice were injected intraperitoneally (i.p.) with 200 μg anti-PD-1 (clone RMP1–14), anti-PSGL-1 (clone 4RA10), or rat IgG (Sigma) isotype control on day 8, 10, and 12 after tumor inoculation ($B16GP_{33}$ and D4M-3A) or day 11, 13, and 15 after tumor inoculation (YUMMER1.7). $CD8^+$ T cells were depleted by intraperitoneal (i.p.) injection of 400 μg anti-mouse Thy1.2 (CD90.2; clone 30H12 from BioXCell), 400 μg anti-mouse Thy1.1 (CD90.1; clone 19E12 from BioXCell), or rat IgG isotype control. Antibodies were injected at day −1, 0, and 3 ($B16\text{-}GP_{33}$) or day −1, 0, 3, and 14 (YUMMer1.7) in respect to tumor inoculation occurring at day 0. The efficacy of depletion was assessed by flow cytometry analysis of retro-orbital blood samples collected on day 8 ($B16\text{-}GP_{33}$) or day 8, 14, and 21 (YUMMER1.7).

Tissue digestion

$B16\text{-}GP_{33}$ tumors were excised, minced, and digested with the gentleMACS™ Octo Dissociator with heaters (Miltenyi Biotec) using the program 37C_m_TDK_1 for 42 minutes with RPM1 and enzyme A and enzyme R from the gentleMACS lung dissociation kit. Digests were then passed through a 70-μm cell strainer, centrifuged at 1200 RPM, washed with RPMI, and then resuspended to generate single-cell suspensions. Spleens were passed through a 70-μm cell strainer, incubated with red blood lysis buffer (Millipore Sigma), and resuspended in Wash Media (Corning HBSS with 2% PSG, 1% FBS, and 0.5% HEPES). Tumor draining lymph nodes were passed through a 70-μm cell strainer and resuspended in Wash Media. Cells were then stained for flow cytometry as described below.

Flow Cytometry

Live spleen, tumor draining lymph nodes, and tumor single-cell suspensions were counted by hemocytometer with trypan blue stain and plated at a concentration of 2×10^6 live cells per well in a U bottom 96 well plate. Plated cells were washed twice with FACS staining buffer (Corning DPBS with 0.5% FBS and 0.5% NaN_3 (stock at 10%)), fixed for 15 minutes with 1% formaldehyde in PBS, washed twice, and resuspended in FACS staining buffer. For intracellular cytokine staining to quantify IFNγ, TNFα, IL2, and granzyme B production, cells were resuspended in complete RPMI-1640 (containing 10 mM HEPES, 1% nonessential amino acids and L-glutamine, 1 mM sodium pyruvate, 10% heat inactivated FBS, and 2% PSG) supplemented with 50 U/mL IL2 (NCI) and 1 mg/mL brefeldin A (BFA, Sigma). Cells were then incubated with phorbol myristate acetate (10 ng/mL) and ionomycin (0.5 μg/mL) at 37°C for 16 hours overnight. Cells were then fixed and permeabilized using a Cytofix/Cytoperm Kit (BD Biosciences) before staining. For intranuclear staining, cells were fixed and permeabilized using a Foxp3 transcription factor fixation/permeabilization kit (Invitrogen) and stained for Ki67 and FOXP3. Antibodies are listed in Suppl. Table S1. Surface stains were performed at a 1:200 dilution, whereas intracellular and intranuclear stains were performed at a 1:100 dilution. All cells were gated with a lymphocyte gate,

followed by two single-cell gates. Activated $CD8^+$ T cells were gated as $CD8^+CD44^{hi}$, and within this population, terminal exhausted cells were gated as $PD\text{-}1^{hi}TIM\text{-}3^{hi}$. $CD4^+$ T cells were gated as $CD4^+CD44^{hi}$ and then divided into $FOXP3^+$ Tregs and $FOXP3^-$ effector cells. Dividing cells in $CD8^+CD44^{hi}$, $CD4^+CD44^{hi}FOXP3^-$, and $CD4^+CD44^{hi}FOXP3^+$ were gated as $Ki67^+$. Cells numbers were calculated by taking $CD8^+CD44^{hi}$, $CD4^+CD44^{hi}FOXP3^-$, or $CD4^+CD44^{hi}FOXP3^+$ frequencies of single cells and multiplying by the total tumor cell counts. Expression was determined by taking the geometric mean of TIM-3, PD-1, LAG3, and PSGL-1 in $CD8^+CD44^{hi}$, $CD4^+CD44^{hi}FOXP3^-$, and $CD4^+CD44^{hi}FOXP3^+$ populations. Representative FACS plots for Treg, Granzyme B, Ki67, and $PD\text{-}1^{hi}TIM\text{-}3^{hi}$ gating are shown in figures where appropriate. FMO and isotype controls are shown in supplement where indicated. All data were collected on a Novocyte 3000 cytometer (Agilent) and analyzed using FlowJo Software (Tree Star).

Tetramer Staining

B16-GP_{33} tumor-derived, single-cell suspensions were stained with a GP_{33} tetramer reagents for 1 hour and 15 minutes at room temperature in complete RPMI-1640, washed twice, fixed for 15 minutes with 1% formaldehyde in PBS, washed twice, and resuspended in FACS staining buffer. A B16-GP_{33} tumor sample stained with all reagents, except for the GP_{33} tetramer, was used as a negative control for tetramer staining. Samples were collected on the Novocyte 3000 cytometer and analyzed with FlowJo Software.

3’ single-cell RNA-sequencing (scRNA-seq) and analyses

WT mice were injected s.c. with 1×10^6 B16-GP_{33} melanoma cells and treated with 200 μg IgG, 200 μg anti-PD-1, 200 μg anti-PSGL-1, or 200 μg each of anti-PSGL-1/anti-PD-1 at 8, 10, and 12 dpi. Tumors were excised and processed at 18 dpi, as indicated above, and immune cells were sorted using propidium iodide (PI) and anti-CD45.2 ($PI^-CD45.2^+$) and processed for 3’ scRNA-seq. Sorted cells were checked for DNA quality and concentration (range 693.9–859.93 pg/μL) and prepared using 10X Genomics Chromium Single-Cell Platforms (Suppl. Table S1), followed by sequencing using an NovaSeq 6000. Raw reads were subjected to quality control analysis with FASTQC software and aligned to the reference transcriptome mm10 using a short-read aligner STAR68 via 10X pipeline cellRanger (v.3.1.0) free open source software available at (https:www.bioinformatics.babraham.ac.uk/projects/fastqc/). The following represent the number of cells obtained per sample processed: IgG (9726 cells), anti-PD-1 (5614 cells), anti-PSGL-1 (7292 cells), and combination (4596 cells). All cells had an average read depth of approximately 18,763 reads per cell, with 2,500 to 3,000 median unique molecular identifiers across approximately 15,000 genes each.

Doublets observed predominantly in larger analyses, particularly the IgG analysis, were identified and removed using Scrublet (32). Expression matrices underwent filtering (nFeature_RNA > 200 and < 5,500 – 6000, percent.mt < 5), normalization, scaling, principle component analysis (PCA), and subsequent UMAP analysis using Seurat packages (33). Resultant Seurat objects were integrated using a CCA (canonical correlation analysis)–based integration method (34). Unique functional cell types were identified by gene expression profiling and queried against Immgen gene expression databases (www.immgen.org) using

the interactive tool “MyGeneSet”. Results were visualized using Seurat FeaturePlot, DotPlot and HeatMap functions. Feature plots and dot plots were generated using Seurat pipeline functions and log-normalized raw counts (data slot). Heatmaps were created using the Seurat DoHeatMap function with log-normalized and scaled raw counts (scale.data slot). All functions were run in the RNA assay. The integrated subsetted $CD8^+$ T-cell Seurat object, containing all 4 conditions, was converted to a SingleCellExperiment (SCE) object for subsequent Slingshot analysis as described (https://rdrr.io/github/kstreet13/bioc2020trajectories/f/vignettes/workshopTrajectories.Rmd (Street, K. 2018)). Cluster 2 (TPEX) was defined as the “start cluster”.

Data and code availability

The authors declare that all supporting data are available within the article and its Supplementary files. 3’ scRNA-seq datasets are deposited in the Gene Expression Omnibus (GEO) database under the accession code: GSE196112.

Quantification and statistical analysis

Data were analyzed using Prism GraphPad software. Analysis was performed using two-tailed *t*-tests or Mann–Whitney *U* tests. Tumor volume growth curves were analyzed by 2-way analysis of variance (ANOVA) with Sidak’s multiple comparisons test (two groups) or 2-way ANOVA with Tukey’s multiple comparisons test (four groups). Survival was analyzed by log-rank (Mantel-Cox) test. Unless otherwise noted, all data are shown as the mean ± SEM.

RESULTS

Selplg is expressed by melanoma tumor-infiltrating immune cells

To determine how PSGL-1 was regulated in tumor-infiltrating immune cells, we implanted wild-type (WT) mice with B16-GP_{33}-expressing melanoma cells (35) and evaluated *Selplg* gene expression at 18 days post injection (dpi) in $CD45.2^+$ sorted cells using 3’ scRNA-seq (Fig. 1A-B). We characterized the tumor-infiltrating $CD45.2^+$ myeloid and non-myeloid immune cells, including macrophages, DCs, neutrophils, T cells, NK cells, and B cells (Fig. 1A, Suppl. Fig. S1, Suppl. Fig. S2A-F). *Selplg* was expressed by subsets of macrophages, DCs, and neutrophils, with very low expression in B cells (Fig. 1B). The highest *Selplg* expression was observed in $CD4^+$ and $CD8^+$ T cells and NK cells (Fig. 1B). We additionally analyzed expression of the PSGL-1 ligands P-selectin (*Selp*) and VISTA (*Vsir*) and detected uniformly low *Selp* expression, whereas high *Vsir* expression was observed in macrophages, neutrophils, and T cells (Fig. 1C-D, Suppl. Fig. S2G-H). These findings showed that although *Selplg* was expressed in most immune cells, the highest expression was observed in T cells and NK cells that infiltrated melanoma tumors.

PSGL-1 is upregulated and co-expressed with immune checkpoints on tumor-infiltrating T cells

Because we found high *Selplg* expression in tumor-infiltrating T cells, we next characterized how PSGL-1 protein expression was regulated during the anti-tumor response. We detected high PSGL-1 expression in effector $CD4^+$ T cells ($CD4^+CD44^+FoxP3^-$), $CD8^+$ T cells

($CD8^+CD44^+$), and Tregs ($CD4^+CD44^+FoxP3^+$) in tumor draining lymph nodes (TdLNs) and significant upregulation in tumors (Fig. 1E-F, Suppl. Fig. S3A). We next determined whether PSGL-1 was co-expressed with additional immune checkpoints and found the majority of tumor-infiltrating $CD8^+$ T cells expressed both PSGL-1 and PD-1, TIM-3, and LAG3 (Fig. 1G, Suppl. Fig. S3B-C). The majority of effector $CD4^+$ T cells and Tregs also had this phenotype, with most tumor infiltrates being $PSGL\text{-}1^+PD\text{-}1^+$, $PSGL\text{-}1^+TIM\text{-}3^+$, and $PSGL\text{-}1^+LAG3^+$ (Fig. 1G, Suppl. Fig. S3B-C). Although T cells in TdLNs expressed PSGL-1, the frequencies of co-inhibitory expression (PD-1, TIM-3, LAG3) were lower compared to the high co-expression found in tumors (Fig. 1G, Suppl. Fig. S3D-E). These findings showed that PSGL-1 had high expression in TdLN T cells and was further upregulated, along with other immune checkpoints, on tumor-infiltrating T cells.

PSGL-1 immune checkpoint targeting changed the melanoma tumor immune landscape

Because we observed *Selplg* expression in various immune cells and PSGL-1 upregulation on all T-cell subsets in melanoma tumors, we next determined whether targeting PSGL-1 and PD-1 in tumor-bearing mice alone or in combination with immune checkpoint blockade could alter tumor growth. We observed large B16-GP_{33} tumors in IgG and anti-PD-1 treated mice and significantly smaller tumors in anti-PSGL-1 and anti-PD-1/anti-PSGL-1 (combination) treated mice (Fig. 2A). We next evaluated the immune cell landscape in these mice by scRNA-seq and identified 18 cell clusters using Immgen (Fig. 2B, Suppl. Fig. S2A-F). We determined changes in cell type frequencies among all four treatment groups. Compared to the IgG and anti-PD-1 groups, the anti-PSGL-1 and combination groups had an increase in neutrophils and T cells, whereas DCs and NK cells were decreased (Fig. 2B-C). Compared to the anti-PD-1 group, the anti-PSGL-1 and combination groups had increased DCs, neutrophils, B cells, and T cells and decreased macrophages and NK cells (Fig. 2B-C).

Because we observed an increase in T cells after anti-PSGL-1 and combination treatments, we further evaluated these clusters independently. We observed six $Cd4^+$ clusters that mapped to Tregs, $CD4^+$ T cells, and $CD4^{lo}$ NKT cells (Fig. 2D-E, Suppl. Fig. S4A-B). Compared to IgG and anti-PD-1 treated tumors, the anti-PSGL-1 and combination groups had decreased Tregs and increased $CD4^+$ T cells (Fig. 2F). Further gene expression profiling revealed that compared to IgG, the anti-PSGL-1 group had decreased expression of inhibitory receptor genes (*Havcr2*, *Lag3*, *Entpd1*, *Cd38*, *Cd101*, *Tigit*, *Ctla4*, *Btla*), increased activation (*Cd69*, *Cd44*, *Cd28*, *Klrg1*) and effector function genes (*Ifng*, *Tnf*, *Il2*, *Cd40lg*, *Bhlhe40*), increased survival genes (*Il2ra*, *Il2*, *Il7r*), and decreased inhibitory genes (*Il10*, *Tgfb1*, *Foxp3*)(Fig. 2G). Many of the inhibitory genes downregulated in anti-PSGL-1 tumors were increased in the anti-PD-1 group, whereas effector genes (*Ifng*, *Tnf*, *Il2*, *Cd40lg*, *Bhlhe40*) were decreased with anti-PD-1 treatment (Fig. 2G).

We next evaluated $Cd8^+$ cells and identified four subclusters (Fig. 2H, Suppl. Fig. S4C-D). Slingshot trajectory analysis showed a developmental trajectory which originated with C2, progressed through C0 and C1, and ended at C3 (Fig. 2H). Most clusters had similar frequencies among treatment groups, except for C2, which was lowest in the anti-PD-1 treated group (Fig. 2I). Based on the trajectory analysis, we next evaluated whether there

were changes in progenitor (Tpex) and terminally (Tex) exhausted T-cell gene signatures in these clusters (Fig. 2J)(36,37). We found that C2 represented the Tpex population, whereas C0, C1, and C3 were terminally exhausted clusters (Fig. 2J). C2 had the highest expression of *Tcf7*, *Slamf6*, *Cd69*, and *Bcl2*, whereas the other clusters had the lowest expression of these genes (Fig. 2J). Following the terminally exhausted trajectory, C0 and C1 had higher *Cd200*, *Havcr2*, *Cd244*, *Cd160*, and *Gzmb* expression (Fig. 2J). Additional global changes in activation and inhibitory markers, as well as transcription factors, were observed within the treatment groups (Suppl. Fig. S4E-F). These findings showed that targeting PSGL-1 alone or in combination with PD-1 in melanoma tumor-bearing mice changed the immune landscape, resulting in decreased Tregs and increased effector $CD4^+$ and $CD8^+$ T-cell gene signatures.

Anti-PSGL-1 and combination treatments increase effector gene signatures in *Cd4*$^+$ and *Cd8*$^+$ T cells

We further evaluated the gene expression patterns in *Cd4*$^+$ clusters within treatment groups (Suppl. Fig. S5A). We observed that compared to IgG, all treatment groups increased *Il10*, *Tgfb1*, *Il2ra*, *Itk*, *Cd28* in Treg clusters (C1 and C3)(Suppl. Fig. S5A). Non-proliferative Tregs (C1) had higher *Klrg1* expression in the anti-PSGL-1 and combination groups, whereas *Klrg1* expression in proliferative Tregs (C3) was highest in the anti-PSGL-1 and anti-PD-1 groups (Suppl. Fig. S5A). *Pdcd1* expression in non-proliferative Tregs was highest in groups treated with anti-PD-1 and combination, yet proliferative Tregs showed the lowest *Pdcd1* in the anti-PD-1 group (Suppl. Fig. S5A). Analysis of the effector *Cd4*$^+$ cell clusters (C0,C2,C4,C5) showed that compared to IgG and anti-PD-1, higher *Il2*, *Tnf*, *Ifng*, *Fasl*, *Itk*, and *Cd28* (except for C5) expression was observed with anti-PSGL-1 and combination treatment (Suppl. Fig. S5A). There were unique changes in gene expression with anti-PSGL-1 treatment, which included higher *Il2*, *Tnf*, *Cd40lg*, and *Cd69* expression in many clusters (Suppl. Fig. S5A). Combination treatment often led to the highest expression of effector genes, even showing synergy in some effector genes (*Il2*, *Tnf*, *Fasl)* (Suppl. Fig. S5A).

We next evaluated the gene expression in *Cd8*$^+$ clusters and observed that compared to IgG, clusters from all three treatments groups had higher *Ifng*, *Prf1*, *Lamp1*, *Fasl*, *Cd28*, *Itk*, *Entpd1*, *Cd44*, *Cd69*, *Havcr2* expression (Suppl. Fig. S5B). Anti-PD-1 treatment led to an upregulation of *Il2* and *Il2ra*, as well as *Cd200* (Suppl. Fig. S5B). Anti-PSGL-1 treatment led to an increase in *Klrg1* and *Slamf6* expression, as well as in the survival genes *Il7r* and *Bcl2* (Suppl. Fig. S5B). The combination treatment group had the highest expression of the effector genes *Tnf, Gzma*, and *Gzmb,* and many clusters showed synergistic expression of *Tnf, Gzma, Gzmb, Itk,* and *Icos. Tox2* was also upregulated in combination treatment clusters (Suppl. Fig. S5B). These findings showed that anti-PSGL-1 monotherapy increased expression of activation and pro-survival genes, whereas the combination treatment resulted in enhanced effector T-cell gene signatures.

PSGL-1 antibody treatment in tumor-bearing mice delays B16-GP$_{33}$ melanoma tumor growth

We next sought to verify our findings from the scRNA-seq analysis by evaluating T-cell changes between WT and anti-PSGL-1 treated mice. WT mice were injected subcutaneously with B16-GP$_{33}$ melanoma tumor cells and at 8 dpi, when tumors were palpable, mice received either IgG or anti-PSGL-1 (Fig. 3A). We found that melanoma tumors grew in IgG treated mice, but tumor growth rate was significantly decreased in anti-PSGL-1 treated mice (Fig. 3B-C). Furthermore, tumors from the anti-PSGL-1 treated mice had lower masses compared to control IgG groups (Fig. 3D). We next examined how anti-PSGL-1 treatment changed the infiltration and activation of T cells within melanoma tumors. We found that anti-PSGL-1 treated mice had a higher frequency of activated CD8$^+$ T cells in tumors, although nearly all the tumor-infiltrating CD8$^+$ T cells were activated with both treatments (Fig. 3E). In contrast, activated CD4$^+$ T-cell frequencies were increased and Treg frequencies were decreased in the tumors of mice that received anti-PSGL-1 treatment (Fig. 3E-F). Because we observed a difference in Tregs, we compared the ratio of effector T cells to Tregs in tumors and found a significant increase in effector T cells compared to Tregs in mice that received PSGL-1 antibody (Fig. 3G-H). Therefore, anti-PSGL-1 therapy in melanoma tumor-bearing mice resulted in tumor control and changed the landscape of T cells that infiltrated these tumors, favoring an increase in effector CD4$^+$ and CD8$^+$ T cells, while decreasing the frequency of Tregs.

PSGL-1 targeting increased effector T-cell responses in melanoma tumors

We next determined the extent that anti-PSGL-1 treatment changed the functionality of the tumor-infiltrating CD4$^+$ and CD8$^+$ T cells. The frequency of granzyme B$^+$ CD8$^+$ T cells was increased in anti-PSGL-1 treated mice compared to CD8$^+$ T cells from IgG treated mice (Fig. 3I-J). We also detected low IFNγ and TNFα production in T cells from IgG treated mice after PMA/Ionomycin re-stimulation, whereas CD4$^+$ and CD8$^+$ T cells in the anti-PSGL-1 treated group had a significantly higher IFNγ and TNFα production (Fig. 3K-M). Our findings showed that anti-PSGL-1 therapy in tumor-bearing mice increased effector functions in tumor-infiltrating CD4$^+$ and CD8$^+$ T cells.

PSGL-1 targeting differentially modulates immune checkpoints on T cells

Because anti-PSGL-1 treatment increased effector functions in anti-tumor T cells, we next evaluated how targeting PSGL-1 modulated immune checkpoint expression in these cells. We observed high PD-1, LAG3, and TIM-3 in CD8$^+$ T cells from IgG treated mice with melanoma tumors (Fig. 4A). CD8$^+$ T cells from tumors of anti-PSGL-1 treated mice had higher surface expression of these immune checkpoints than IgG treated mice (Fig. 4A, Suppl. Fig. S6A). In contrast to CD8$^+$ T cells, CD4$^+$ T cells from tumors of anti-PSGL-1 treated mice had no difference in PD-1 expression, but didi have decreased TIM-3 and LAG3 expression (Fig. 4B, Suppl. Fig. S6B). Like effector CD4$^+$ T cells, Tregs also expressed similarly high PD-1 in IgG and anti-PSGL-1 treated mice (Fig. 4C, Suppl. Fig. S6C). In contrast to CD4$^+$ and CD8$^+$ T cells, Tregs had no difference in expression levels of TIM-3 and LAG3 between IgG and anti-PSGL-1 treated mice (Fig. 4C, Suppl. Fig. S6C). These data showed that although all T cells in tumors expressed high PSGL-1, PSGL-1

targeting differentially changed expression of inhibitory receptors in $CD4^+$ and $CD8^+$ T cells, but not in Tregs.

Terminally exhausted $CD8^+$ T cells are increased after anti-PSGL-1 treatment

Because we observed increased expression of immune checkpoints in $CD8^+$ T cells from anti-PSGL-1 treated mice, we next evaluated whether terminally vs progenitor exhausted T-cell subsets were different among treatment groups. We observed an increased frequency of terminally exhausted ($PD\text{-}1^{hi}TIM\text{-}3^+$) $CD8^+$ T cells and decreased frequency of progenitor exhausted ($PD\text{-}1^{int}TIM\text{-}3^-$) $CD8^+$ T cells in tumors after anti-PSGL-1 treatment (Fig. 4D-E). We also detected a population of $PD\text{-}1^-TIM\text{-}3^-$ $CD8^+$ T cells that was decreased in anti-PSGL-1 treated mice (Fig. 4D-E). Terminally exhausted T cells, which retain cytotoxic function, are increased after anti-PD-1 immune checkpoint therapy (38–40). We observed that terminally exhausted T cells proliferated more than progenitor exhausted T cells in both treatment groups, as shown by higher $Ki67^+$ cells (Suppl. Fig. S6D). We observed increased proliferation in the $PD\text{-}1^-TIM\text{-}3^-$ population from anti-PSGL-1 treated mice (Suppl. Fig. S6D), despite their lower frequencies in the anti-PSGL-1 treated mice (Fig. 4D). Ki67 may last longer in cells than the period of proliferation; therefore, the increased Ki67 in the $PD\text{-}1^-TIM\text{-}3^-$ population could indicate more rapid differentiation into the terminal state. Because the proliferative burst after anti-PD-1 treatment resulted in the accumulation of the $PD\text{-}1^{hi}TIM\text{-}3^+$ population, we examined whether anti-PSGL-1 treatment changed the absolute number of these T cells within tumors. We detected an increase in the accumulation of these terminally exhausted $CD8^+$ T cells in melanoma tumors after anti-PSGL-1 treatment (Fig. 4F). Because our earlier findings showed a decrease in Tregs after anti-PSGL-1 treatment, we evaluated whether the PSGL-1 antibody (clone 4RA10 IgG_1) depleted cells *in vivo*. We found no depletion of Tregs, $CD4^+$, or $CD8^+$ T cells in spleen or lymph nodes in anti-PSGL-1 treated mice (Suppl. Fig. S6E). These findings indicate that after anti-PSGL-1 treatment, there is an increase in the presence of terminally exhausted ($PD\text{-}1^{hi}TIM\text{-}3^+$) T cells in tumors.

Targeting PSGL-1 with PD-1 blockade promotes anti-tumor immunity to melanoma

We next assessed the efficacy of combination therapy with antibodies targeting PSGL-1 and PD-1 in B16-GP_{33} tumor-bearing mice (Suppl. Fig. S7A) and frequencies of activated T cells in tumors. We found that the majority of $CD8^+$ T cells in tumors were $CD44^+$, with a small increase in activated $CD8^+$ T cells in mice treated with anti-PSGL-1 and combination therapy (Fig. 5A). We observed increased frequencies of $CD4^+$ T cells in mice that received anti-PSGL-1 monotherapy and combination therapy compared to IgG or anti-PD-1 treated mice (Fig. 5A). Although we observed a large Treg infiltrate in tumors from IgG and anti-PD-1 treated mice, anti-PSGL-1 monotherapy and combination therapy both caused a significant decrease in frequency of Tregs (Fig. 5A). Furthermore, we found an increased ratio of effector $CD4^+$ and $CD8^+$ T cells to Tregs in mice treated with anti-PSGL-1 and combination therapy compared to IgG treated mice (Fig. 5B-C). We next determined if antibody therapy affected T-cell proliferation in tumors and found that compared to IgG, anti-PD-1 treatment increased $CD8^+$ but not $CD4^+$ T-cell proliferation, as measured by Ki67 (Fig. 5D-E). We did detect, however, a significant increase in $Ki67^+$ $CD8^+$ and $CD4^+$ T cells after both anti-PSGL-1 monotherapy and combination therapy (Fig. 5D-E). We detected

increased proliferation in T cells from anti-PSGL-1 treated mice, and the combination therapy had similar results, showing no further increase from the addition of anti-PD-1 (Fig. 5D-E). To determine how combination therapy changed T-cell function, we evaluated granzyme B in $CD8^+$ T cells (Fig. 5F-G). We found similar frequencies of granzyme B^+ $CD8^+$ T cells in tumors from IgG and anti-PD-1 treated mice and increased frequencies after anti-PSGL-1 monotherapy and combination therapy (Fig. 5F-G). We again did not detect enhanced granzyme B production when anti-PD-1 was combined with anti-PSGL-1 treatment. Although we saw increased anti-tumor immunity with anti-PSGL-1 treatment in experiments performed with B16-GP_{33} melanoma cells, tumors eventually grew in all treatment groups, and mice had to be euthanized. However, we observed the highest median survival at 18 dpi in mice treated with combination therapy (Fig. 5H). These findings showed that anti-PSGL-1 therapy improved anti-tumor immunity in melanoma tumors that were largely unresponsive to PD-1 therapy.

Antigen-specific $CD8^+$ T cells are increased relative to Tregs in tumors after antibody targeting of PSGL-1

We next quantified the number of T cells infiltrating tumors and found increased infiltration of $CD8^+$ and $CD4^+$ T cells in anti-PSGL-1 treated mice compared to IgG control (Fig. 6A). We observed similar numbers of Tregs in IgG and anti-PD-1 treated mice but found a significant decrease in anti-PSGL-1 and combination treated mice (Fig. 6B). No differences in Treg numbers in tumors were observed between mice receiving anti-PSGL-1 monotherapy or combination therapy (Fig. 6B). We next examined the frequencies of antigen-specific $CD8^+$ T cells by staining with MHC class I tetramer specific for the GP_{33} peptide expressed by B16-GP_{33} melanoma. We found similar frequencies of $GP_{33}{}^+CD8^+$ T cells in IgG and anti-PD-1 treated mice, a significant increase in the frequency of $GP_{33}{}^+$ $CD8^+$ T cells in anti-PSGL-1 treated mice, and a trend towards increased frequency in combination treated mice compared to IgG (Fig. 6C-D). We observed no differences in the numbers of $GP_{33}{}^+CD8^+$ T cells per gram of tumor among treatment groups (Fig. 6C). We quantified the ratio of $GP_{33}{}^+CD8^+$ T cells to Tregs in tumors and found a significant increase in $GP_{33}{}^+CD8^+$ T cells compared to Tregs in anti-PSGL-1 and combination treated mice compared to IgG and anti-PD-1 treated mice (Fig. 6E). To assess the role of T cells in this model, we next depleted T cells in tumor-bearing mice that received immune checkpoint antibody therapy (Suppl. Fig. S7B). We found no differences in tumor volume or mass in any of the antibody treated groups (Suppl. Fig. S7C-D). We next evaluated the efficacy of anti-PSGL-1 treatment in a different melanoma tumor model. We treated WT mice harboring D4M-3A tumors with anti-PSGL-1 and found a significant decrease in tumor volume and mass compared to IgG treated mice (Fig. 6F-G). These findings showed increased ratio of tumor-infiltrating, antigen-specific $CD8^+$ T cells to Tregs after anti-PSGL-1 and combination treatment. Anti-PSGL-1 treatment also slowed D4M-3A melanoma tumor growth, which like B16-GP_{33}, is also an aggressive tumor resistant to anti-PD-1 treatment (41).

PSGL-1 deficiency with anti-PD-1 treatment promotes melanoma tumor control

We next determined whether immune checkpoint therapy could be combined with PSGL-1 deficiency to promote melanoma tumor control. We injected WT and *Selplg*$^{-/-}$ mice

subcutaneously with YUMMER1.7 melanoma cells, a highly immunogenic, anti-PD-1 sensitive cell line (Fig. 7A)(42) and treated with either IgG or anti-PD-1 when tumors were measurable. We found that WT IgG treated mice developed tumors that continued to increase in size (Fig. 7B-C). WT anti-PD-1 treated mice also developed tumors and average tumor volume was similar to IgG treated mice (Fig. 7B-C). In contrast, *Selplg*$^{-/-}$ mice treated with IgG had significantly smaller tumors compared to WT IgG or anti-PD-1 treated mice (Fig. 7B-C). Furthermore, when *Selplg*$^{-/-}$ mice were injected with anti-PD-1, they demonstrated the most robust tumor control of all four groups examined, eliminating their tumors by 24 dpi (Fig. 7B-C). Despite some small tumors present in some WT IgG treated mice, none (0/6) controlled their tumors, whereas WT anti-PD-1 treated mice (2/6) showed tumor control (Fig. 7D). In contrast, a portion of *Selplg*$^{-/-}$ IgG treated mice (3/6) eliminated tumors, whereas all *Selplg*$^{-/-}$ anti-PD-1 treated mice (6/6) eradicated their tumors (Fig. 7D). To demonstrate the robustness of this phenotype, we combined tumor control data from three independent experiments. We determined complete responses (CR) leading to tumor clearance in 0/18 (0%) WT IgG, 4/18 (22%) WT anti-PD-1, 4/19 (21%) *Selplg*$^{-/-}$ IgG, and 13/20 (65%) in *Selplg*$^{-/-}$ anti-PD-1 treated mice (Fig. 7E). Although some *Selplg*$^{-/-}$ anti-PD-1 treated mice had tumors, the tumors never reached the larger volumes observed in the IgG or anti-PD-1 treatment groups (Fig. 7E). To confirm the role of T cells in the observed phenotypes, we depleted T cells in WT and *Selplg*$^{-/-}$ mice before anti-PD-1 therapy and observed tumor growth, with no tumor clearance in all mouse groups by 28 dpi (Fig. 7F-G). These findings showed that although *Selplg*$^{-/-}$ mice had better tumor control than WT mice, combining PSGL-1 deficiency with PD-1 blockade resulted in the highest frequency of tumor-free mice.

DISCUSSION

In this study, we targeted PSGL-1 in tumor-bearing mice and uncovered an increased anti-tumor T-cell response in the tumor microenvironment, which slowed melanoma tumor growth and increased the activation of effector $CD4^+$ and $CD8^+$ T cells in tumors. T cells from anti-PSGL-1 treated mice had increased effector functions, proliferation, and were essential in delaying tumor growth after antibody treatment. We found that targeting PSGL-1 decreased the frequencies of Tregs in tumors, resulting in an increased presence of effector T cells. We assessed whether combination treatment further improved anti-tumor responses in WT mice and found that targeting PSGL-1 and PD-1 resulted in smaller tumors compared to IgG controls, and combination therapy had a similar efficacy to anti-PSGL-1 monotherapy. Even though combination therapy did not eliminate the poorly immunogenic B16-GP_{33} cell line, we did find complete responses when *Selplg*$^{-/-}$ tumor-bearing mice were given anti-PD-1 therapy using the more immunogenic YUMMER1.7 cell line.

It is well established that immune checkpoints are upregulated on exhausted T cells in tumors and inhibit T-cell effector functions (43). Although most immune checkpoints are induced upon T-cell activation, PSGL-1 is constitutively expressed on T cells. However, PSGL-1 expression does increase significantly as T cells move from the TdLNs into the tumor microenvironment. Although PSGL-1 was expressed on all tumor-infiltrating T cells, expression differed in $CD4^+$ and $CD8^+$ T cells, and Tregs, with Tregs expressing the highest levels. Furthermore, most T cells in melanoma tumors co-expressed PSGL-1 and additional

immune checkpoints (PD-1, TIM-3, LAG3). This suggests potential co-regulation of these inhibitory receptors and possible cooperation in promoting the T-cell exhaustion state. Indeed, *Selplg*$^{-/-}$ T cells in melanoma tumors are shown to have decreased PD-1, TIM-3, and LAG3 (11). Our findings suggest that these varying PSGL-1 levels in tumor-infiltrating T cells may result in different phenotypic and functional changes as these cells respond to tumor antigens. This concept is supported by our observations of increased PD-1, TIM-3, and LAG3 on CD8$^+$ T cells, decreased TIM-3 and LAG3 on CD4$^+$ T cells, and unchanged immune checkpoint expression in Tregs from anti-PSGL-1 treated mice. Although CD8$^+$ T cells expressed higher immune checkpoints after PSGL-1 targeting, these levels are proposed by others to indicate T-cell activation (44). Furthermore, it was recently shown that exhausted CD8$^+$ T cells increase their PD-1 expression and TCR signaling after anti-PD-L1 blockade *in vivo* (45). Anti-tumor CD8$^+$ T cells responding to PD-1 checkpoint blockade have increased frequencies of the exhausted terminal PD-1^{hi}TIM-3$^+$ population, seeded by proliferation of progenitor exhausted T cells (36). Although this is a terminally exhausted population, these T cells retain effector functions that promote tumor killing (36). Like PD-1 blockade, we found that after anti-PSGL-1 treatment, PD-1^{hi}TIM-3$^+$ CD8$^+$ T cells were enriched in tumors, indicating that this population may be key in promoting tumor killing. This conclusion was supported by the increased IFNγ, TNFα, and granzyme B production, increased proliferation, and the increased T-cell activation gene signatures we observed in CD8$^+$ T cells in tumors from anti-PSGL-1 treated mice. CD4$^+$ T cells had decreased TIM-3 and LAG3 immune checkpoint expression and were more functional in anti-PSGL-1 treated mice, suggesting improved help to CD8$^+$ T cells during therapy, as CD4$^+$ T-cell help is critical in melanoma tumor control (46,47). Indeed, our scRNA-seq analyses showed improved CD4$^+$ T-cell helper functions after anti-PSGL-1 treatment.

The cellular mechanisms that promote melanoma tumor control during anti-PSGL-1 treatment require T cells, as shown by our studies in which T cell-depleted mice treated with anti-PSGL-1 antibodies had no observable tumor control. Although we found that T cells were critical in mediating melanoma tumor control, it is possible that additional immune cells may also be modulated after anti-PSGL-1 therapy. Others have shown that *Selplg*$^{-/-}$ DCs are more stimulatory and that PSGL-1 signaling can induce tolerogenic DCs that support Tregs (26). Future studies will address how anti-PSGL-1 therapy alters the differentiation and function of additional immune cells in the melanoma tumor microenvironment to support an improved anti-tumor T-cell response.

Our finding that Treg frequencies were decreased in melanoma tumors after anti-PSGL-1 therapy further highlights the inhibitory role of Tregs in limiting effector T-cell responses. Studies have shown that depleting Tregs in melanoma tumors can promote tumor rejection (48), and the ratio of Tregs to effector T cells increases in growing tumors (49). Decreasing Tregs in murine and human cancers has been suggested to predict immunotherapy efficacy (50–52). We found decreased Tregs and increased effector T cells after anti-PSGL-1 treatment. These findings suggest that a more pro-inflammatory environment was present in tumors from anti-PSGL-1 treated mice. Our findings that anti-PSGL-1 treatment reinvigorated CD4$^+$ and CD8$^+$ T-cell proliferation in tumors supports the concept that targeting PSGL-1 can relieve Treg-mediated inhibition. This was further supported by our scRNA-seq analysis showing upregulated activation and effector genes in *Cd4*$^+$ and

Cd8^{+} cells after anti-PSGL-1 treatment. Important for therapeutic purposes, these immune changes occurred after melanoma tumors were already palpable in mice, indicating that reducing Tregs in established tumors is attainable when PSGL-1 is targeted.

Melanoma is a very aggressive cancer and until recently, patients with metastatic disease had few treatment options and most died within months of diagnosis (53). Immune checkpoint blockade therapies, such as anti-PD-1 and anti-CTLA-4 treatment, have saved the lives of patients worldwide, but many continue to be unresponsive to these therapies (54). Although the human disease differs from melanoma in animal models, preclinical studies have been key in testing the efficacy of new approaches to reinvigorate T cells in tumors. We injected highly immunogenic YUMMER1.7 melanoma cells into mice and discovered that *Selplg*$^{-/-}$ mice had better tumor control than WT IgG or WT anti-PD-1 treated mice. When tumor-bearing *Selplg*$^{-/-}$ mice were additionally injected with anti-PD-1, these mice showed complete responses, with many mice eliminating their tumors. These findings mirror clinical findings showing that immune checkpoint blockade therapies are more effective in patients with highly mutated melanomas (55). Our findings in *Selplg*$^{-/-}$ mice underscore the relevance of combining PSGL-1 inhibition with PD-1 blockade as a new strategy to promote tumor control.

Our studies using the highly aggressive B16 melanoma model revealed that anti-PSGL-1 antibody therapy was effective in slowing melanoma growth through mechanisms leading to increased T-cell activation, proliferation, and effector functions. B16 melanomas have been reported to be resistant to anti-PD-1 and anti-PD-L1 therapy (56,57), and we found that anti-PSGL-1 treatment in tumor-bearing mice could delay B16 tumor growth. We also observed delayed D4M-3A melanoma tumor growth in anti-PSGL-1 treated mice, an additional melanoma cell line resistant to anti-PD-1 therapy (41). When we combined therapies in B16-tumor bearing mice by injecting them with anti-PSGL-1 and anti-PD-1, we observed no enhancement of T-cell effector phenotypes. However, the combination treatment increased the medial overall survival of these mice. Whereas our work focused on targeting PSGL-1 to promote anti-tumor immunity, others have shown tumor control through blockade of known PSGL-1 ligands, such as the recently identified VISTA ligand (58–60). Our scRNA-seq showed that most immune cells in melanoma had low to undetectable P-selectin (*Selp*) expression, but they did express high VISTA (*Vsir*). The PSGL-1 antibody (4RA10 clone) has been shown to block P-selectin binding (61), but because more *Vsir* than *Selp* is present in cells in the tumor microenvironment, our data suggest that VISTA-PSGL-1 binding may be a dominant interaction. It is also possible that additional PSGL-1 binding partners may contribute to PSGL-1-dependent inhibition in the tumor draining lymph node and/or the tumor microenvironment. Our findings showing that anti-PSGL-1 treatment was effective against anti-PD-1/anti-PD-L1 resistant B16-GP_{33} and D4M-3A melanomas indicate that targeting PSGL-1 may represent a new therapeutic approach to control tumors that are unresponsive to standard therapies.

We showed that PSGL-1 is highly expressed and upregulated on T cells in the melanoma tumor microenvironment and is co-expressed with multiple immune checkpoints on exhausted T cells and Tregs. Given the importance of immune checkpoint blockade therapies that reinvigorate T cells in tumors, it is significant that anti-PSGL-1 therapy

in mice harboring aggressive B16-GP_{33} and D4M-3A melanomas delayed tumor growth. Furthermore, combining anti-PD-1 therapy in PSGL-1-deficient mice showed complete responses in mice harboring highly mutated YUMMER1.7 melanomas. Our findings identify PSGL-1 as an immune checkpoint target and suggest that inhibiting this pathway may provide new treatment options with the possibility of eliciting anti-tumor immunity in patients with cancer.

Supplementary Material

Refer to Web version on PubMed Central for supplementary material.

ACKNOWLEDGMENTS

We would like to thank all the current and former members in the Tinoco Laboratory (Twitter: @Tinoco_Lab) for all their constructive comments and advice during this project. We would like to thank Dr. David Fruman and Dr. Francesco Marangoni for critical review of our manuscript (UC Irvine). We would like to thank Melinda Gormley (UC Irvine) for editing our manuscript. This work was supported by the National Institutes of Health (R01 AI13723 to R.T.), Department of Defense (W81XWH-18-1-0738 to R.T.), The Melanoma Research Alliance (571135 to R.T.), and in part by (American Cancer Society Institutional Research Grant IRG-16-187-13 to R.T.) from the American Cancer Society, T32 Training Program for Interdisciplinary Cancer Research IDCR (T32CA009054 to J.M.D.), NIH IMDS training grant (GM055246 to K.M.V.), T32 Microbiology and Infectious Diseases training grant (T32AI141346 to K.M.V.), and T32 virus-host interactions: a multi-scale training program (T32AI007319 to E.N.N.). C.F.G-J. is supported by UC Irvine Chancellor's ADVANCE Postdoctoral Fellowship Program, NSF-Simons Postdoctoral Fellowship, and NSF Grant DMS1763272 (to Qing Nie), and a kind gift from the Howard Hughes Medical Institute Hanna H. Gray Postdoctoral Fellowship Program. The authors would like to thank Dr. Denise Gay (DLG Biologics) for assistance processing scRNA-seq data and Dr. Jie Wu and Dr. Melanie Oakes (UCI Genomics High Throughput Facility) for setup and analysis of scRNA-seq, which is a Chao Family Comprehensive Cancer Center (CFCCC) shared resource supported by the Cancer Center Support Grant (P30CA062203).

REFERENCES

1. Khalil DN, Smith EL, Brentjens RJ, Wolchok JD. The future of cancer treatment: immunomodulation, CARs and combination immunotherapy. Nat Rev Clin Oncol 2016;13(6):394 doi 10.1038/nrclinonc.2016.65. [PubMed: 27118494]
2. Topalian SL, Hodi FS, Brahmer JR, Gettinger SN, Smith DC, McDermott DF, et al. Safety, activity, and immune correlates of anti-PD-1 antibody in cancer. N Engl J Med 2012;366(26):2443–54 doi 10.1056/NEJMoa1200690. [PubMed: 22658127]
3. Brahmer JR, Tykodi SS, Chow LQ, Hwu WJ, Topalian SL, Hwu P, et al. Safety and activity of anti-PD-L1 antibody in patients with advanced cancer. N Engl J Med 2012;366(26):2455–65 doi 10.1056/NEJMoa1200694. [PubMed: 22658128]
4. Hodi FS, O'Day SJ, McDermott DF, Weber RW, Sosman JA, Haanen JB, et al. Improved survival with ipilimumab in patients with metastatic melanoma. N Engl J Med 2010;363(8):711–23 doi 10.1056/NEJMoa1003466. [PubMed: 20525992]
5. Hamid O, Robert C, Daud A, Hodi FS, Hwu WJ, Kefford R, et al. Safety and tumor responses with lambrolizumab (anti-PD-1) in melanoma. N Engl J Med 2013;369(2):134–44 doi 10.1056/NEJMoa1305133. [PubMed: 23724846]
6. Ramos-Casals M, Brahmer JR, Callahan MK, Flores-Chavez A, Keegan N, Khamashta MA, et al. Immune-related adverse events of checkpoint inhibitors. Nat Rev Dis Primers 2020;6(1):38 doi 10.1038/s41572-020-0160-6. [PubMed: 32382051]
7. Topalian SL, Sznol M, McDermott DF, Kluger HM, Carvajal RD, Sharfman WH, et al. Survival, durable tumor remission, and long-term safety in patients with advanced melanoma receiving nivolumab. J Clin Oncol 2014;32(10):1020–30 doi 10.1200/JCO.2013.53.0105. [PubMed: 24590637]

8. Wolchok JD, Kluger H, Callahan MK, Postow MA, Rizvi NA, Lesokhin AM, et al. Nivolumab plus ipilimumab in advanced melanoma. N Engl J Med 2013;369(2):122–33 doi 10.1056/NEJMoa1302369. [PubMed: 23724867]
9. Galli F, Aguilera JV, Palermo B, Markovic SN, Nistico P, Signore A. Relevance of immune cell and tumor microenvironment imaging in the new era of immunotherapy. J Exp Clin Cancer Res 2020;39(1):89 doi 10.1186/s13046-020-01586-y. [PubMed: 32423420]
10. Hashimoto M, Kamphorst AO, Im SJ, Kissick HT, Pillai RN, Ramalingam SS, et al. CD8 T Cell Exhaustion in Chronic Infection and Cancer: Opportunities for Interventions. Annu Rev Med 2018;69:301–18 doi 10.1146/annurev-med-012017-043208. [PubMed: 29414259]
11. Tinoco R, Carrette F, Barraza ML, Otero DC, Magana J, Bosenberg MW, et al. PSGL-1 Is an Immune Checkpoint Regulator that Promotes T Cell Exhaustion. Immunity 2016;44(5):1190–203 doi 10.1016/j.immuni.2016.04.015. [PubMed: 27192578]
12. Levesque JP, Zannettino AC, Pudney M, Niutta S, Haylock DN, Snapp KR, et al. PSGL-1-mediated adhesion of human hematopoietic progenitors to P-selectin results in suppression of hematopoiesis. Immunity 1999;11(3):369–78 doi 10.1016/s1074-7613(00)80112-0. [PubMed: 10514015]
13. Rossi FM, Corbel SY, Merzaban JS, Carlow DA, Gossens K, Duenas J, et al. Recruitment of adult thymic progenitors is regulated by P-selectin and its ligand PSGL-1. Nat Immunol 2005;6(6):626–34 doi 10.1038/ni1203. [PubMed: 15880112]
14. Sultana DA, Zhang SL, Todd SP, Bhandoola A. Expression of functional P-selectin glycoprotein ligand 1 on hematopoietic progenitors is developmentally regulated. J Immunol 2012;188(9):4385–93 doi 10.4049/jimmunol.1101116. [PubMed: 22461691]
15. Johnston RJ, Su LJ, Pinckney J, Critton D, Boyer E, Krishnakumar A, et al. VISTA is an acidic pH-selective ligand for PSGL-1. Nature 2019;574(7779):565–70 doi 10.1038/s41586-019-1674-5. [PubMed: 31645726]
16. Pepin M, Mezouar S, Pegon J, Muczynski V, Adam F, Bianchini EP, et al. Soluble Siglec-5 associates to PSGL-1 and displays anti-inflammatory activity. Sci Rep 2016;6:37953 doi 10.1038/srep37953.
17. Veerman KM, Williams MJ, Uchimura K, Singer MS, Merzaban JS, Naus S, et al. Interaction of the selectin ligand PSGL-1 with chemokines CCL21 and CCL19 facilitates efficient homing of T cells to secondary lymphoid organs. Nat Immunol 2007;8(5):532–9 doi 10.1038/ni1456. [PubMed: 17401367]
18. Veldkamp CT, Kiermaier E, Gabel-Eissens SJ, Gillitzer ML, Lippner DR, DiSilvio FA, et al. Solution Structure of CCL19 and Identification of Overlapping CCR7 and PSGL-1 Binding Sites. Biochemistry 2015;54(27):4163–6 doi 10.1021/acs.biochem.5b00560. [PubMed: 26115234]
19. Abadier M, Ley K. P-selectin glycoprotein ligand-1 in T cells. Curr Opin Hematol 2017;24(3):265–73 doi 10.1097/MOH.0000000000000331. [PubMed: 28178038]
20. Yang J, Hirata T, Croce K, Merrill-Skoloff G, Tchernychev B, Williams E, et al. Targeted gene disruption demonstrates that P-selectin glycoprotein ligand 1 (PSGL-1) is required for P-selectin-mediated but not E-selectin-mediated neutrophil rolling and migration. J Exp Med 1999;190(12):1769–82 doi 10.1084/jem.190.12.1769. [PubMed: 10601352]
21. Perez-Frias A, Gonzalez-Tajuelo R, Nunez-Andrade N, Tejedor R, Garcia-Blanco MJ, Vicente-Rabaneda E, et al. Development of an autoimmune syndrome affecting the skin and internal organs in P-selectin glycoprotein ligand 1 leukocyte receptor-deficient mice. Arthritis Rheumatol 2014;66(11):3178–89 doi 10.1002/art.38808. [PubMed: 25132671]
22. Angiari S, Rossi B, Piccio L, Zinselmeyer BH, Budui S, Zenaro E, et al. Regulatory T cells suppress the late phase of the immune response in lymph nodes through P-selectin glycoprotein ligand-1. J Immunol 2013;191(11):5489–500 doi 10.4049/jimmunol.1301235. [PubMed: 24174617]
23. He X, Schoeb TR, Panoskaltsis-Mortari A, Zinn KR, Kesterson RA, Zhang J, et al. Deficiency of P-selectin or P-selectin glycoprotein ligand-1 leads to accelerated development of glomerulonephritis and increased expression of CC chemokine ligand 2 in lupus-prone mice. J Immunol 2006;177(12):8748–56 doi 10.4049/jimmunol.177.12.8748. [PubMed: 17142777]

24. Nunez-Andrade N, Lamana A, Sancho D, Gisbert JP, Gonzalez-Amaro R, Sanchez-Madrid F, et al. P-selectin glycoprotein ligand-1 modulates immune inflammatory responses in the enteric lamina propria. J Pathol 2011;224(2):212–21 doi 10.1002/path.2850. [PubMed: 21432853]
25. Yoshizaki A, Yanaba K, Iwata Y, Komura K, Ogawa A, Akiyama Y, et al. Cell adhesion molecules regulate fibrotic process via Th1/Th2/Th17 cell balance in a bleomycin-induced scleroderma model. J Immunol 2010;185(4):2502–15 doi 10.4049/jimmunol.0901778. [PubMed: 20624949]
26. Urzainqui A, Martinez del Hoyo G, Lamana A, de la Fuente H, Barreiro O, Olazabal IM, et al. Functional role of P-selectin glycoprotein ligand 1/P-selectin interaction in the generation of tolerogenic dendritic cells. J Immunol 2007;179(11):7457–65 doi 10.4049/jimmunol.179.11.7457. [PubMed: 18025190]
27. Spertini C, Baisse B, Spertini O. Ezrin-radixin-moesin-binding sequence of PSGL-1 glycoprotein regulates leukocyte rolling on selectins and activation of extracellular signal-regulated kinases. J Biol Chem 2012;287(13):10693–702 doi 10.1074/jbc.M111.318022.
28. Urzainqui A, Serrador JM, Viedma F, Yanez-Mo M, Rodriguez A, Corbi AL, et al. ITAM-based interaction of ERM proteins with Syk mediates signaling by the leukocyte adhesion receptor PSGL-1. Immunity 2002;17(4):401–12 doi 10.1016/s1074-7613(02)00420-x. [PubMed: 12387735]
29. Tinoco R, Neubert EN, Stairiker CJ, Henriquez ML, Bradley LM. PSGL-1 Is a T Cell Intrinsic Inhibitor That Regulates Effector and Memory Differentiation and Responses During Viral Infection. Front Immunol 2021;12:677824 doi 10.3389/fimmu.2021.677824.
30. Veerman KM, Carlow DA, Shanina I, Priatel JJ, Horwitz MS, Ziltener HJ. PSGL-1 regulates the migration and proliferation of CD8(+) T cells under homeostatic conditions. J Immunol 2012;188(4):1638–46 doi 10.4049/jimmunol.1103026. [PubMed: 22250093]
31. Matsumoto M, Miyasaka M, Hirata T. P-selectin glycoprotein ligand-1 negatively regulates T-cell immune responses. J Immunol 2009;183(11):7204–11 doi 10.4049/jimmunol.0902173. [PubMed: 19890058]
32. Wolock SL, Lopez R, Klein AM. Scrublet: Computational Identification of Cell Doublets in Single-Cell Transcriptomic Data. Cell Syst 2019;8(4):281–91 e9 doi 10.1016/j.cels.2018.11.005. [PubMed: 30954476]
33. Butler A, Hoffman P, Smibert P, Papalexi E, Satija R. Integrating single-cell transcriptomic data across different conditions, technologies, and species. Nat Biotechnol 2018;36(5):411–20 doi 10.1038/nbt.4096. [PubMed: 29608179]
34. Stuart T, Butler A, Hoffman P, Hafemeister C, Papalexi E, Mauck WM 3rd, et al. Comprehensive Integration of Single-Cell Data. Cell 2019;177(7):1888–902 e21 doi 10.1016/j.cell.2019.05.031. [PubMed: 31178118]
35. Janelle V, Langlois MP, Tarrab E, Lapierre P, Poliquin L, Lamarre A. Transient complement inhibition promotes a tumor-specific immune response through the implication of natural killer cells. Cancer Immunol Res 2014;2(3):200–6 doi 10.1158/2326-6066.CIR-13-0173. [PubMed: 24778316]
36. Miller BC, Sen DR, Al Abosy R, Bi K, Virkud YV, LaFleur MW, et al. Subsets of exhausted CD8(+) T cells differentially mediate tumor control and respond to checkpoint blockade. Nat Immunol 2019;20(3):326–36 doi 10.1038/s41590-019-0312-6. [PubMed: 30778252]
37. Andreatta M, Corria-Osorio J, Muller S, Cubas R, Coukos G, Carmona SJ. Interpretation of T cell states from single-cell transcriptomics data using reference atlases. Nat Commun 2021;12(1):2965 doi 10.1038/s41467-021-23324-4. [PubMed: 34017005]
38. Blackburn SD, Shin H, Freeman GJ, Wherry EJ. Selective expansion of a subset of exhausted CD8 T cells by alphaPD-L1 blockade. Proc Natl Acad Sci U S A 2008;105(39):15016–21 doi 10.1073/pnas.0801497105.
39. Mognol GP, Spreafico R, Wong V, Scott-Browne JP, Togher S, Hoffmann A, et al. Exhaustion-associated regulatory regions in CD8(+) tumor-infiltrating T cells. Proc Natl Acad Sci U S A 2017;114(13):E2776-E85 doi 10.1073/pnas.1620498114.
40. Paley MA, Kroy DC, Odorizzi PM, Johnnidis JB, Dolfi DV, Barnett BE, et al. Progenitor and terminal subsets of CD8+ T cells cooperate to contain chronic viral infection. Science 2012;338(6111):1220–5 doi 10.1126/science.1229620. [PubMed: 23197535]

41. Di Pilato M, Kim EY, Cadilha BL, Prussmann JN, Nasrallah MN, Seruggia D, et al. Targeting the CBM complex causes Treg cells to prime tumours for immune checkpoint therapy. Nature 2019;570(7759):112–6 doi 10.1038/s41586-019-1215-2. [PubMed: 31092922]
42. Wang J, Perry CJ, Meeth K, Thakral D, Damsky W, Micevic G, et al. UV-induced somatic mutations elicit a functional T cell response in the YUMMER1.7 mouse melanoma model. Pigment Cell Melanoma Res 2017;30(4):428–35 doi 10.1111/pcmr.12591. [PubMed: 28379630]
43. Barrueto L, Caminero F, Cash L, Makris C, Lamichhane P, Deshmukh RR. Resistance to Checkpoint Inhibition in Cancer Immunotherapy. Transl Oncol 2020;13(3):100738 doi 10.1016/j.tranon.2019.12.010.
44. Wei SC, Duffy CR, Allison JP. Fundamental Mechanisms of Immune Checkpoint Blockade Therapy. Cancer Discov 2018;8(9):1069–86 doi 10.1158/2159-8290.CD-18-0367. [PubMed: 30115704]
45. Sandu I, Cerletti D, Claassen M, Oxenius A. Exhausted CD8(+) T cells exhibit low and strongly inhibited TCR signaling during chronic LCMV infection. Nat Commun 2020;11(1):4454 doi 10.1038/s41467-020-18256-4. [PubMed: 32901001]
46. Zander R, Schauder D, Xin G, Nguyen C, Wu X, Zajac A, et al. CD4(+) T Cell Help Is Required for the Formation of a Cytolytic CD8(+) T Cell Subset that Protects against Chronic Infection and Cancer. Immunity 2019;51(6):1028–42 e4 doi 10.1016/j.immuni.2019.10.009. [PubMed: 31810883]
47. DeRogatis JM, Viramontes KM, Neubert EN, Tinoco R. PSGL-1 Immune Checkpoint Inhibition for CD4(+) T Cell Cancer Immunotherapy. Front Immunol 2021;12:636238 doi 10.3389/fimmu.2021.636238.
48. Kline J, Brown IE, Zha YY, Blank C, Strickler J, Wouters H, et al. Homeostatic proliferation plus regulatory T-cell depletion promotes potent rejection of B16 melanoma. Clin Cancer Res 2008;14(10):3156–67 doi 10.1158/1078-0432.CCR-07-4696. [PubMed: 18483384]
49. Ahmetlic F, Riedel T, Homberg N, Bauer V, Trautwein N, Geishauser A, et al. Regulatory T Cells in an Endogenous Mouse Lymphoma Recognize Specific Antigen Peptides and Contribute to Immune Escape. Cancer Immunol Res 2019;7(4):600–8 doi 10.1158/2326-6066.CIR-18-0419. [PubMed: 30894379]
50. Gambichler T, Schroter U, Hoxtermann S, Susok L, Stockfleth E, Becker JC. Decline of programmed death-1-positive circulating T regulatory cells predicts more favourable clinical outcome of patients with melanoma under immune checkpoint blockade. Br J Dermatol 2020;182(5):1214–20 doi 10.1111/bjd.18379. [PubMed: 31361026]
51. Ko K, Yamazaki S, Nakamura K, Nishioka T, Hirota K, Yamaguchi T, et al. Treatment of advanced tumors with agonistic anti-GITR mAb and its effects on tumor-infiltrating Foxp3+CD25+CD4+ regulatory T cells. J Exp Med 2005;202(7):885–91 doi 10.1084/jem.20050940. [PubMed: 16186187]
52. Liakou CI, Kamat A, Tang DN, Chen H, Sun J, Troncoso P, et al. CTLA-4 blockade increases IFNgamma-producing CD4+ICOShi cells to shift the ratio of effector to regulatory T cells in cancer patients. Proc Natl Acad Sci U S A 2008;105(39):14987–92 doi 10.1073/pnas.0806075105.
53. Larkin J, Chiarion-Sileni V, Gonzalez R, Grob JJ, Rutkowski P, Lao CD, et al. Five-Year Survival with Combined Nivolumab and Ipilimumab in Advanced Melanoma. N Engl J Med 2019;381(16):1535–46 doi 10.1056/NEJMoa1910836. [PubMed: 31562797]
54. Nowicki TS, Hu-Lieskovan S, Ribas A. Mechanisms of Resistance to PD-1 and PD-L1 Blockade. Cancer J 2018;24(1):47–53 doi 10.1097/PPO.0000000000000303. [PubMed: 29360728]
55. Kim JY, Kronbichler A, Eisenhut M, Hong SH, van der Vliet HJ, Kang J, et al. Tumor Mutational Burden and Efficacy of Immune Checkpoint Inhibitors: A Systematic Review and Meta-Analysis. Cancers (Basel) 2019;11(11) doi 10.3390/cancers11111798.
56. Kleffel S, Posch C, Barthel SR, Mueller H, Schlapbach C, Guenova E, et al. Melanoma Cell-Intrinsic PD-1 Receptor Functions Promote Tumor Growth. Cell 2015;162(6):1242–56 doi 10.1016/j.cell.2015.08.052. [PubMed: 26359984]
57. Lin H, Wei S, Hurt EM, Green MD, Zhao L, Vatan L, et al. Host expression of PD-L1 determines efficacy of PD-L1 pathway blockade-mediated tumor regression. J Clin Invest 2018;128(2):805–15 doi 10.1172/JCI96113. [PubMed: 29337305]

58. Mehta N, Maddineni S, Kelly RL, Lee RB, Hunter SA, Silberstein JL, et al. An engineered antibody binds a distinct epitope and is a potent inhibitor of murine and human VISTA. Sci Rep 2020;10(1):15171 doi 10.1038/s41598-020-71519-4.

59. Rosenbaum SR, Knecht M, Mollaee M, Zhong Z, Erkes DA, McCue PA, et al. FOXD3 Regulates VISTA Expression in Melanoma. Cell Rep 2020;30(2):510–24 e6 doi 10.1016/j.celrep.2019.12.036. [PubMed: 31940493]

60. Wang L, Rubinstein R, Lines JL, Wasiuk A, Ahonen C, Guo Y, et al. VISTA, a novel mouse Ig superfamily ligand that negatively regulates T cell responses. J Exp Med 2011;208(3):577–92 doi 10.1084/jem.20100619. [PubMed: 21383057]

61. Pendl GG, Robert C, Steinert M, Thanos R, Eytner R, Borges E, et al. Immature mouse dendritic cells enter inflamed tissue, a process that requires E- and P-selectin, but not P-selectin glycoprotein ligand 1. Blood 2002;99(3):946–56 doi 10.1182/blood.v99.3.946. [PubMed: 11806998]

Synopsis:

Therapeutic PSGL-1 antibody targeting increases infiltration, activation, and function of $CD4^+$ and $CD8^+$ T cells in melanoma tumors, leading to improved tumor control and altered tumor immune landscape that includes decreased Tregs and increased antigen-specific T cells.

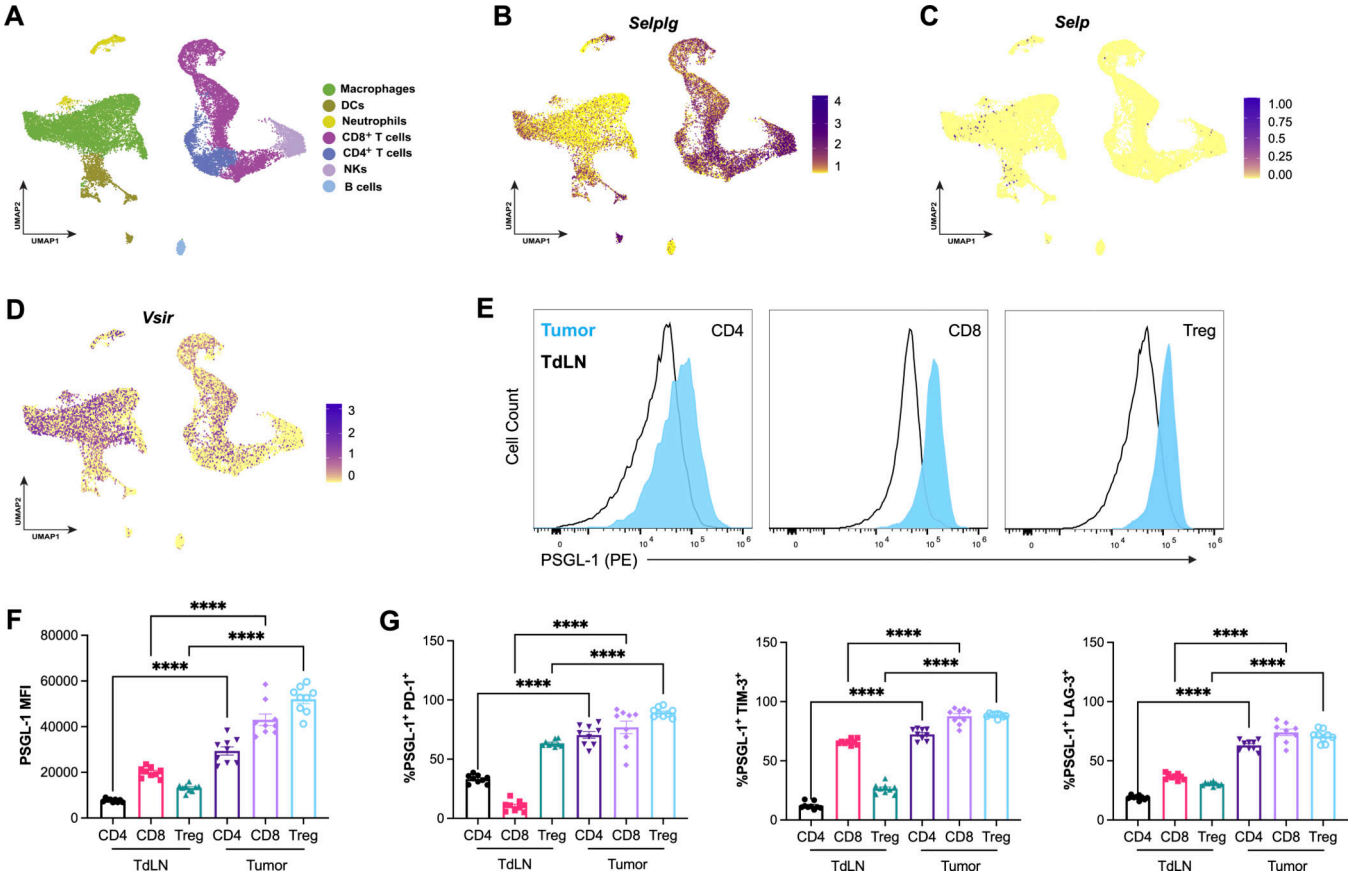

Figure 1: PSGL-1 expression in tumor-infiltrating T cells.

WT mice were injected s.c with B16-GP_{33} (1×10^6) melanoma cells, and tumors and TdLNs were isolated at 18 dpi and tumors assessed via scRNA-seq. (**A**) Integration of Seurat clustering analysis of sorted CD45.2$^+$ immune cells isolated from B16-GP_{33} melanoma tumors projected in UMAP with color-coded cluster identities. Integrated Seurat immune cell clusters with relative (**B**) *Selplg*, (**C**) *Selp*, and (**D**) *Vsir* expression are shown. Yellow indicates low and Purple indicates high expression. (**E-F**) The mean fluorescence intensity (MFI) of PSGL-1 on CD4$^+$, CD8$^+$ and Tregs in the tumor and TdLNs is shown and quantified. (**G**) PSGL-1 co-expression with PD-1, TIM-3, and LAG3 is shown for CD4$^+$, CD8$^+$ and Tregs in TdLNs and tumors. Data are representative of three independent experiments (n≥ 8 mice/group) and show the mean±SEM. *P< 0.05, **P< 0.005, ***P< 0.001, ****P< 0.0001 by ordinary one-way ANOVA with Tukey's multiple comparisons test.

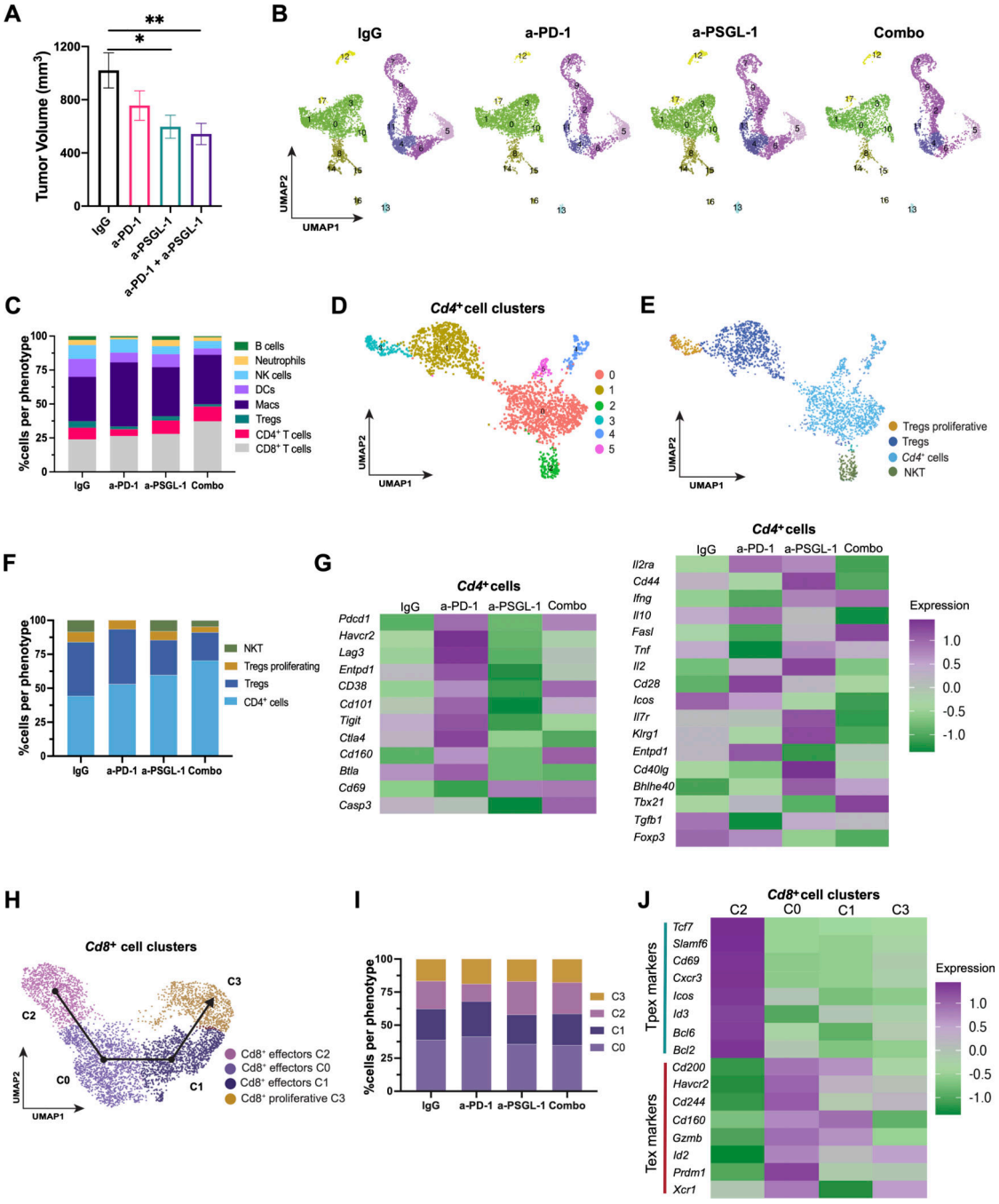

Figure 2: Immune cell changes in tumors after immune checkpoint blockade.

WT mice were injected s.c. with (1×10^6) B16-GP_{33} melanoma cells and treated with IgG or anti-PSGL-1 at 8, 10, and 12 dpi. (**A**) B16-GP_{33} tumor volume at 18 dpi is shown for IgG, anti-PD-1, anti-PSGL-1, and combination anti-PD-1/anti-PSGL-1-treated mice. Tumors were harvested and assess via scRNA-seq at 18 dpi. (**B**) Seurat clustering analysis of sorted $CD45.2^+$ immune cells projected in two-dimensional UMAP with color-coded cluster identities. (**C**) Stacked bar graphs of immune cell frequencies derived from Seurat cluster analysis are shown for each treatment group. Seurat subset clustering analysis of

(**D**) *Cd4*$^{+}$ immune cells with (**E**) color coded identities. (**F**) Stacked bar graph showing Tregs, proliferating Treg, NKT, and CD4^{+} T-cell frequencies in each treatment group. (**G**) Heatmaps displaying relative expression of the indicated inhibitory and effector genes in *Cd4*$^{+}$ subset clusters from all four treatment groups. (**H**) Seurat subset clustering of *Cd8*$^{+}$ cells with slingshot cluster trajectory (black arrow) and (**I**) corresponding stacked bar graphs of *Cd8*$^{+}$ cluster frequencies for all four treatment groups. (**J**) Heatmaps displaying relative expression of T-cell precursor exhausted (Tpex) or terminally exhausted (Tex) genes in *Cd8*$^{+}$ subset clusters from all four treatment groups.

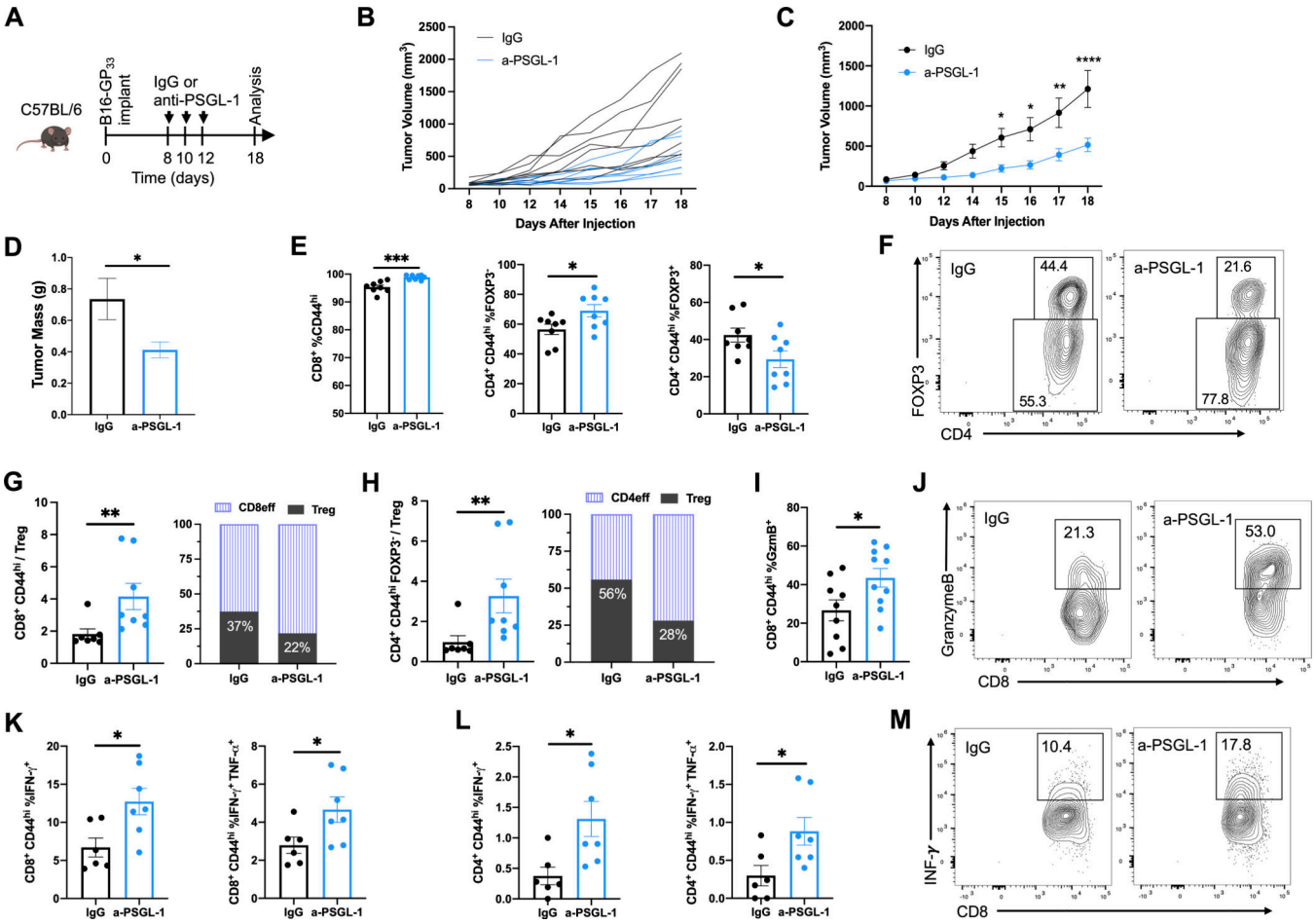

Figure 3: WT mice treated with anti-PSGL-1 have improved tumor immunity.

(**A**) WT mice were injected s.c. with (1×10^6) B16-GP_{33} melanoma cells and treated with IgG or anti-PSGL-1 at 8, 10, and 12 dpi. (**B-C**) Tumor volume and (**D**) tumor mass at 18 dpi. Tumors were harvested and analyzed by flow cytometry at 18 dpi. (**E**) Frequencies of tumor-infiltrating T cells and (**F**) representative FACS plots of Tregs. (**G-H**) Ratio of T cell subsets to Tregs in tumors. (**I**) Frequency of granzyme B^+ $CD8^+$ T cells in the tumor and (**J**) representative FACS plots. (**K-L**) Frequency of cytokine producing $CD8^+$ and $CD4^+$ T cells and (**M**) representative FACS plots. Data are representative of four independent experiments (n≥8 mice/group). Graphs show the mean±SEM. *P< 0.05, **P< 0.005, ***P< 0.001, ****P< 0.0001 by 2-way ANOVA with Sidak's multiple comparisons test (tumor growth curve) or two-tailed t-test or Mann–Whitney U test.

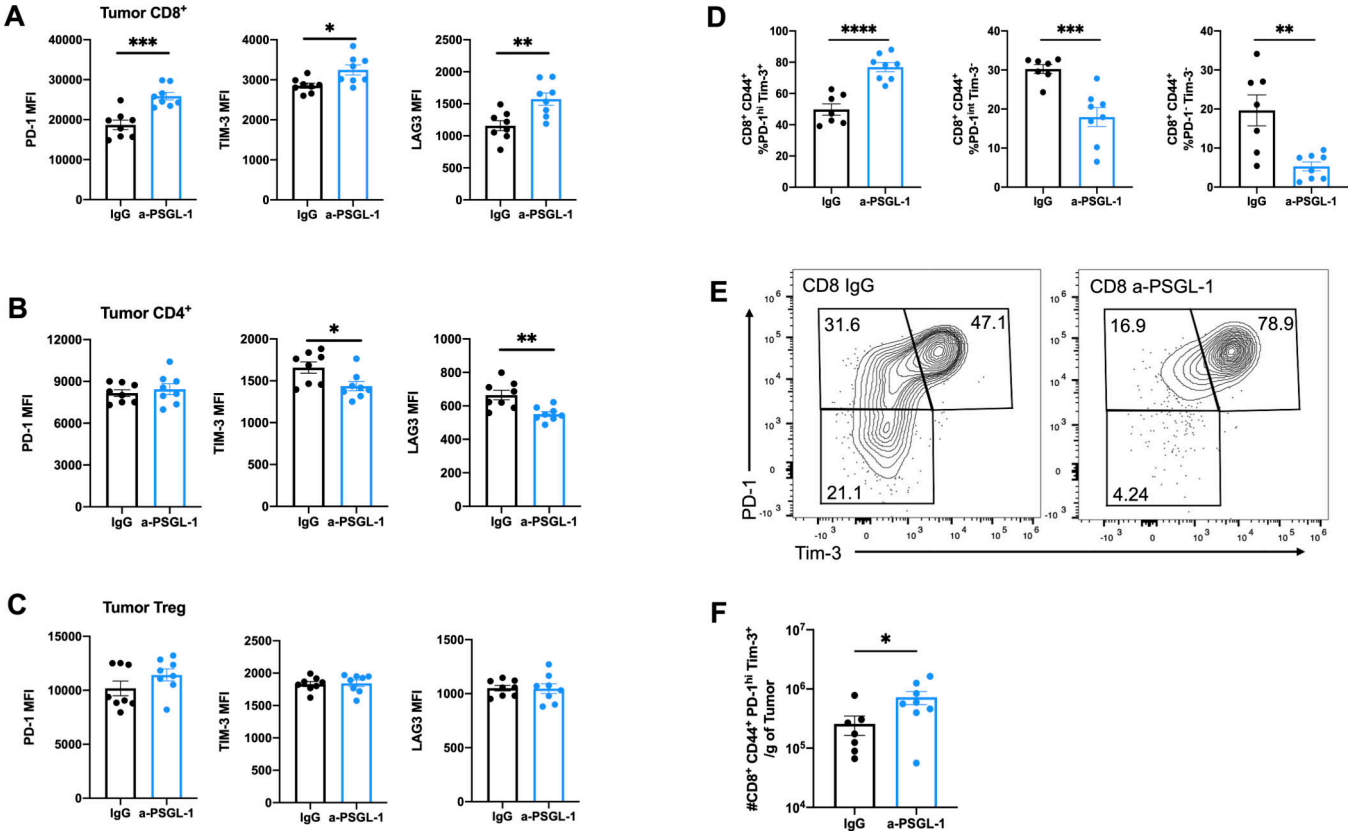

Figure 4: Activated CD8$^+$ T cells are increased in tumors after anti-PSGL-1 therapy.

WT mice were injected s.c. with (1×10^6) B16-GP$_{33}$ melanoma cells and treated with IgG or anti-PSGL-1 at 8, 10, and 12 dpi, and tumors were isolated at 18 dpi and analyzed via flow cytometry. (**A**) PD-1, TIM-3, and LAG3 mean fluorescence intensity (MFI) on CD8$^+$ T cells, (**B**) CD4$^+$ T cells, and (**C**) Tregs in tumors. (**D**) CD8$^+$ T-cell populations in tumors were phenotyped as terminally exhausted (PD-1^{hi}TIM-3$^+$), progenitor exhausted (PD-1^{int}TIM-3$^-$), and PD-1$^-$TIM-3$^-$ and (**E**) representative FACS plots are shown. Quadrants were set using isotype controls. (**F**) The number of CD8$^+$ PD-1^{hi}TIM-3$^+$ T cells per gram of tumor. Data are representative of four independent experiments (n≥8 mice/group). Graphs show the mean±SEM. *P< 0.05, **P< 0.005, ***P< 0.001, ****P< 0.0001 by two-tailed t-test or Mann–Whitney U test.

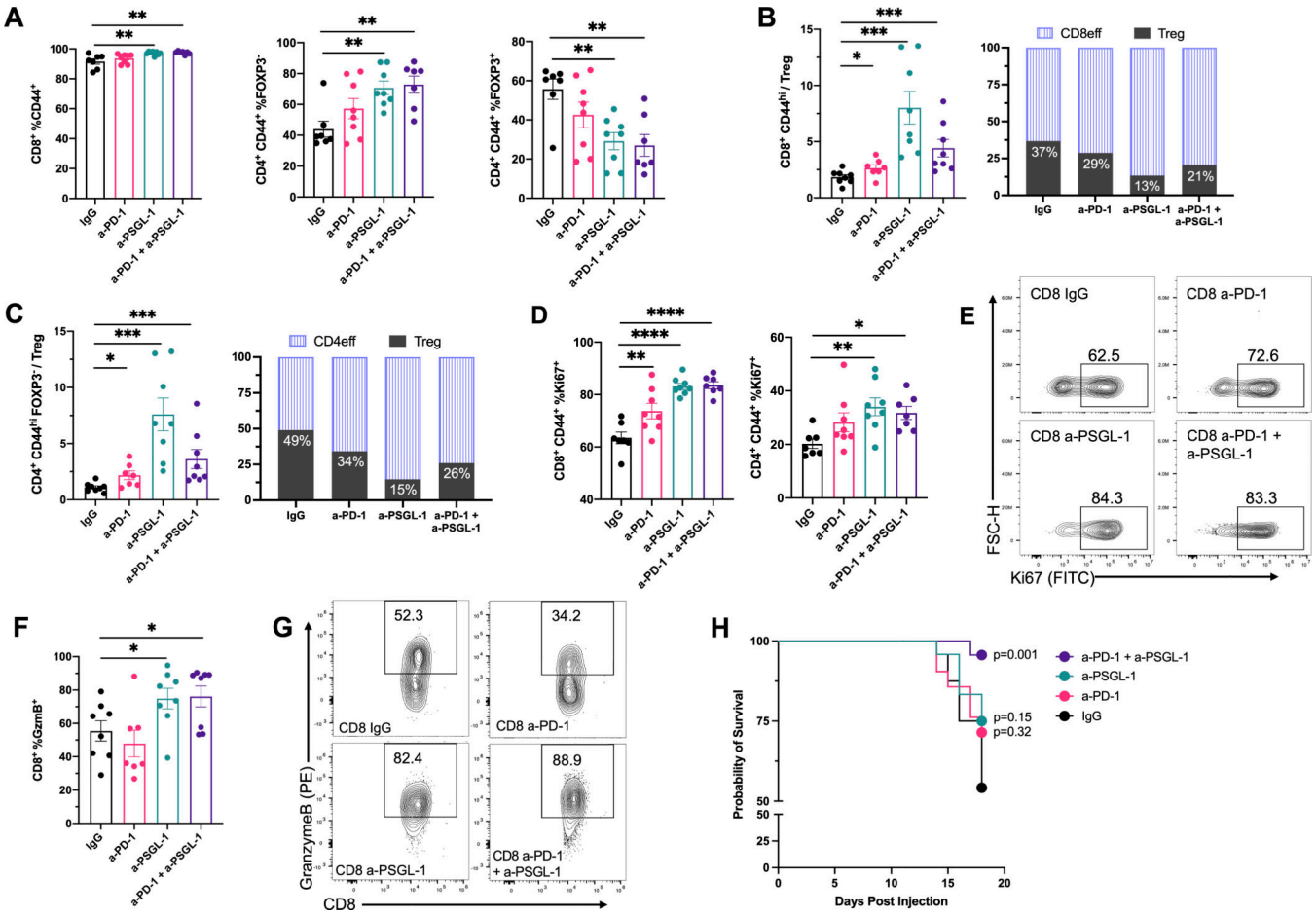

Figure 5: Tumor immune responses after anti-PSGL-1 and anti-PD-1 combination therapy.

WT mice were injected s.c. with (1×10^6) B16-GP_{33} melanoma cells and treated with IgG, anti-PD-1, anti-PSGL-1, or both anti-PD-1 and anti-PSGL-1 at 8, 10, and 12 dpi. Tumors were isolated at 18 dpi, and (**A**) frequencies of activated ($CD44^+$) $CD8^+$ and $CD4^+$, T cells, Tregs and (**B-C**) the ratio of $CD4^+$ and $CD8^+$ effector to Tregs are shown. (**D,E**) Frequencies of $Ki67^+$ T cells and representative FACS plots for $CD8^+$ T cells. (**F**) Frequencies of granzyme B^+ $CD8^+$ T cells and (**G**) representative FACS plots. (**H**) Survival curve of IgG, anti-PD-1, anti-PSGL-1, or both anti-PD-1 and anti-PSGL-1-treated mice up to 18 dpi. Data are representative of four independent experiments (n≥7 mice/group). Graphs show the mean±SEM. *P< 0.05, **P< 0.005, ***P< 0.001, ****P< 0.0001 by two-tailed t-test or Mann–Whitney U test (tumor mass) or log-rank (Mantel-Cox) test (survival).

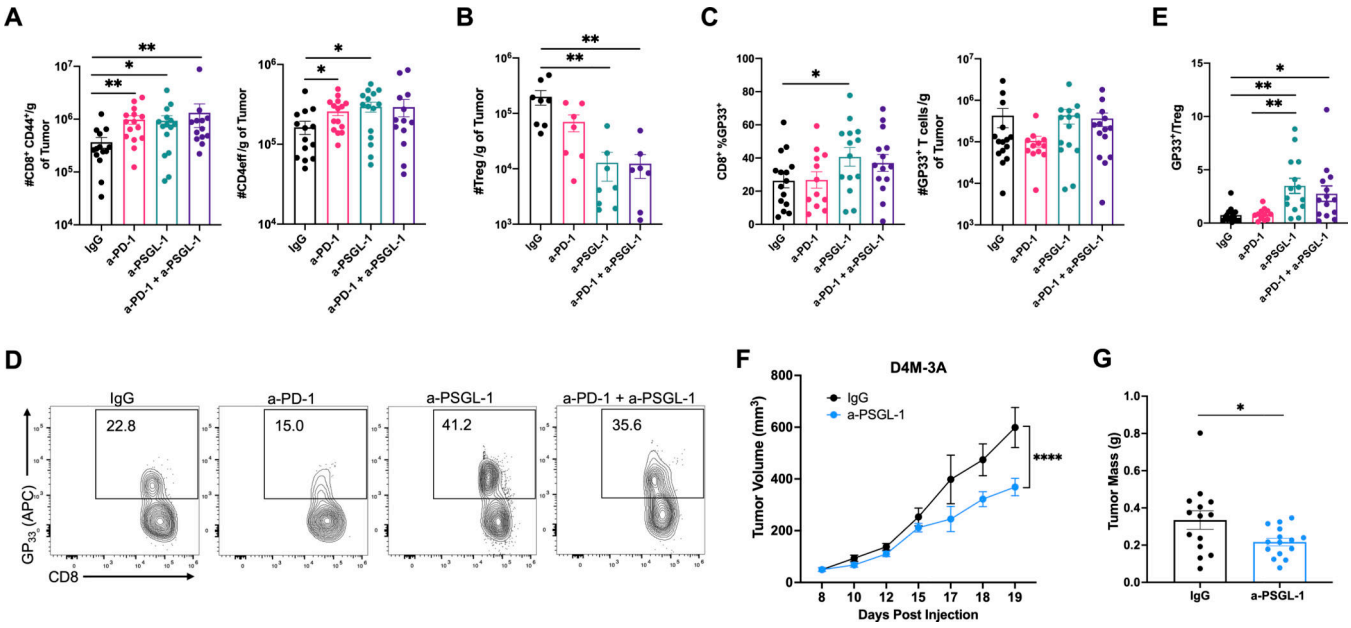

Figure 6: Tumor-specific CD8$^+$ T cells and Tregs after anti-PD-1/anti-PSGL-1 combination therapy.

WT mice were injected with (1×10^6) B16-GP$_{33}$ melanoma cells s.c. and injected with IgG, anti-PD-1, anti-PSGL-1, or anti-PD-1/anti-PSGL-1 at 8, 10, and 12 dpi. Tumors were harvested and assessed via flow cytometry at 18 dpi. (**A**) The number of CD8$^+$, CD4$^+$ T cells, and (**B**) Tregs per gram of tumor at 18 dpi. (**C**) The frequencies and numbers of GP$_{33}^+$CD8$^+$ T cells per gram of tumor. (**D**) Representative FACs plots showing the frequency of tetramer$^+$(GP$_{33}^+$)CD8$^+$ T cells in tumors. (**E**) The ratio of GP$_{33}^+$CD8$^+$ T cells to Tregs in tumors. (**F-G**) WT mice were injected with (1×10^6) D4M-3A melanoma cells s.c. and injected with IgG or anti-PSGL-1 antibodies at 8, 10, and 12 dpi. (**F**) Tumor volume and (**G**) tumor mass are shown at 19 dpi. Data are representative of four (**A-B**) or two (**C-G**) independent experiments (n≥5 mice/group). Graphs show the mean±SEM. *P< 0.05, **P< 0.005, ***P< 0.001 by two-tailed t-test or Mann–Whitney U test or by 2-way ANOVA with Sidak's multiple comparisons test (tumor growth curve).

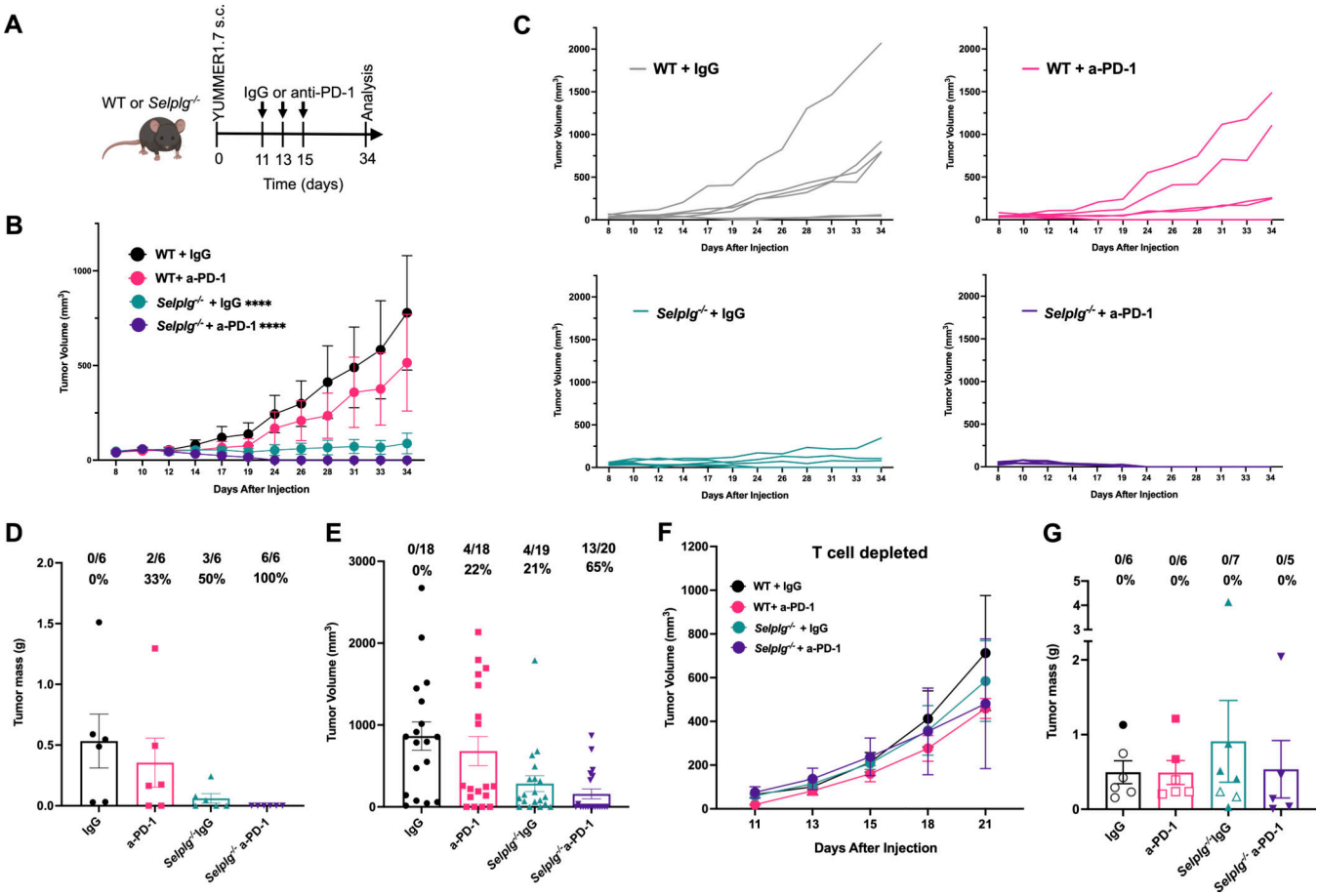

Figure 7: PD-1 blockade in *Selplg*$^{-/-}$ mice promotes complete responses to melanoma.

(**A**) WT and *Selplg*$^{-/-}$ mice were injected s.c. with (2×10^6) YUMMER1.7 melanoma cells and then treated with IgG or anti-PD-1, or with T-cell depleting antibodies and IgG or anti-PD-1 at the indicated times. (**B-C**) Tumor volume over time. (**D**) Quantification of tumor mass at 34 dpi and (**E**) tumor volumes. Tumor volumes are representative of three combined experiments. (**F-G**) Quantification of tumor volume over time, and tumor mass in T cell-depleted mice. (**G**) Mice euthanized at 21 dpi (open symbols) or 28 dpi (filled symbols). Data are representative of three combined independent experiments in (A-E)(n≥6 mice/group, endpoints 34 and 38dpi) or one experiment in (F-G)(n≥ 6 mice/group, endpoint 28dpi). Fraction of mice without tumors at the end of each experiment are shown at (D-E) 34 dpi and (G) 21 dpi (open symbols) or 28 dpi (filled symbols). Graphs show the mean±SEM. *P< 0.05, **P< 0.005, ***P< 0.001, ****P< 0.0001 as determined by 2-way ANOVA with Tukey's multiple comparisons test (tumor volume growth curve).